nature protocols

PROTOCOL

https://doi.org/10.1038/s41596-019-0132-z

Nanoscale chemical imaging using tip-enhanced Raman spectroscopy

Naresh Kumar[1,2], Bert M. Weckhuysen[2], Andrew J. Wain[1] and Andrew J. Pollard[1*]

Confocal and surface-enhanced Raman spectroscopy (SERS) are powerful techniques for molecular characterization; however, they suffer from the drawback of diffraction-limited spatial resolution. Tip-enhanced Raman spectroscopy (TERS) overcomes this limitation and provides chemical information at length scales in the tens of nanometers. In contrast to alternative approaches to nanoscale chemical analysis, TERS is label free, is non-destructive, and can be performed in both air and liquid environments, allowing its use in a diverse range of applications. Atomic force microscopy (AFM)-based TERS is especially versatile, as it can be applied to a broad range of samples on various substrates. Despite its advantages, widespread uptake of this technique for nanoscale chemical imaging has been inhibited by various experimental challenges, such as limited lifetime, and the low stability and yield of TERS probes. This protocol details procedures that will enable researchers to reliably perform TERS imaging using a transmission-mode AFM-TERS configuration on both biological and non-biological samples. The procedure consists of four stages: (i) preparation of plasmonically active TERS probes; (ii) alignment of the TERS system; (iii) experimental procedures for nanoscale imaging using TERS; and (iv) TERS data processing. We provide procedures and example data for a range of different sample types, including polymer thin films, self-assembled monolayers (SAMs) of organic molecules, photocatalyst surfaces, small molecules within biological cells, single-layer graphene and single-walled carbon nanotubes in both air and water. With this protocol, TERS probes can be prepared within ~23 h, and each subsequent TERS experimental procedure requires 3–5 h.

Introduction

Understanding the impact of nanostructure on the macroscopic chemical behavior of surfaces plays a vital role in the design, development and implementation of new functional materials, including solid catalysts, adsorbants, membranes, sensors and components for photovoltaic devices. However, conventional analytical techniques often lack the required sensitivity to detect the features of interest, and/or the spatial resolution to isolate them and establish their distribution across the sample. Raman spectroscopy is one such tool that can provide detailed chemical information by measuring vibrational modes of analyte molecules. However, it suffers from the limitations of low sensitivity and a diffraction-limited spatial resolution (typically 200–300 nm). Meanwhile, scanning probe microscopy (SPM) techniques, such as AFM and scanning tunneling microscopy (STM), can yield topography information with up to atomic resolution but typically fail to provide chemical insights.

The sensitivity and spatial resolution of Raman spectroscopy can be markedly improved by employing the localized surface plasmon resonance (LSPR) effect, in which a high-intensity and localized electric field is generated at the surface of a metal nanoparticle illuminated by light matching its natural plasmon frequency. This phenomenon is exploited in TERS, which has emerged as a powerful nanoanalytical tool for nanoscale chemical characterization over the past 2 decades[1–4]. TERS harnesses a combination of LSPR and the lightning rod effect to generate an enhanced electromagnetic (EM) field at the apex of a sharp metallic SPM probe positioned in the focal spot of an excitation laser (Fig. 1a)[5]. This EM field enhancement can reach several orders of magnitude and is localized to a region similar in dimensions to the probe apex (typically <50 nm), as demonstrated by the simulated map shown in Fig. 1b[1,6]. Together with chemical enhancement effects in some cases[7], these phenomena result in an increase in Raman scattering signal intensity from molecules present in the vicinity of the probe apex and allow TERS to overcome the diffraction and sensitivity limitations of conventional Raman spectroscopy. Thus, TERS combines the high chemical sensitivity of SERS

[1]National Physical Laboratory, Teddington, UK. [2]Inorganic Chemistry and Catalysis Group, Debye Institute for Nanomaterials Science, Utrecht University, Utrecht, the Netherlands. *e-mail: andrew.pollard@npl.co.uk

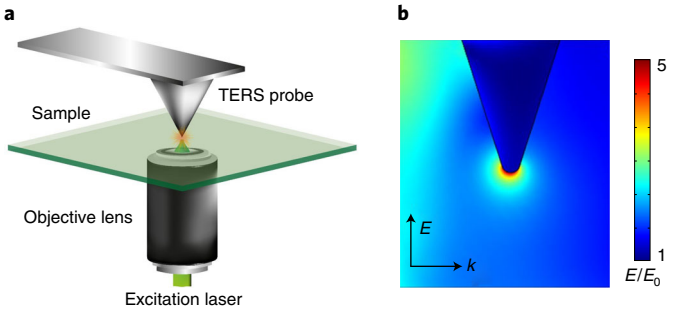

Fig. 1 | TERS principle. a, Schematic diagram illustrating the principle of TERS, combining the chemical sensitivity of SERS and the high lateral resolution of SPM. **b**, Simulated electric field amplitude map of an Ag TERS probe apex irradiated with a laser of 532-nm wavelength with an electric field parallel to the probe axis calculated using COMSOL Multiphysics. *k* indicates the wave vector of the excitation laser. Probe apex radius: 15 nm. Note that this simulation model, which consists of a metallic probe in contact with a dielectric substrate, greatly simplifies the real TERS experimental conditions, for example, by ignoring the surface roughness of the TERS probe, plasmonic interaction between the probe apex and the substrate, focusing of the laser using a high-numerical-aperture objective lens, and the radial polarization of the excitation laser typically used in a bottom-up illumination geometry. Therefore, the electric field enhancement values obtained from TERS experiments may often be higher than those predicted by numerical simulations[29]. **b** adapted from Kumar et al.[29] under a Creative Commons Attribution 4.0 license (https://creativecommons.org/licenses/by/4.0/legalcode).

and the high spatial resolution of SPM, thereby providing non-destructive and label-free surface chemical imaging at nanometer length scales.

Despite the apparent simplicity of the TERS principle, its experimental implementation remains highly challenging, which is reflected by the fact that only a handful of academic groups have actually reported successful and consistent TERS measurements, despite commercial systems being available. This is largely because TERS demands experimental expertise across a range of differing scientific disciplines, including metal thin-film deposition, laser optical alignment, plasmonics, confocal Raman spectroscopy and SPM. This protocol provides detailed, practical guidance on tackling the various obstacles in order to enable more widespread uptake of this important analytical technique. We specifically focus on TERS performed in combination with AFM, although many of the principles are transferrable to STM-based TERS.

Overview of the procedure

This protocol is divided into four parts, each of which addresses a key aspect of nanoscale chemical imaging using TERS. Metal-coated probes are the most critical component of a TERS experiment. Therefore, the procedure for TERS probe preparation is addressed in part 1, which consists of four essential steps: oxidation of Si AFM probes, cleaning of oxidized AFM probes, metal deposition and assessment of TERS probe quality (Steps 1–11).

Once plasmonically active TERS probes have been prepared, the TERS system needs to be optimized before measurements. This is addressed in part 2, which details procedures for laser alignment of the microscope, alignment of the TERS probes with the excitation laser, locating the near-field 'hotspot' at the TERS probe apex and confirming the quality of the near-field hotspot (Steps 12–40).

After the TERS system and TERS probes are ready, a wide range of samples can be measured. In part 3, we describe procedures for using TERS for measurements of a polymer thin film on glass, a SAM of an organic molecule on Au, monitoring of a photocatalytic reaction, nanoscale imaging of single-layer graphene, imaging of phospholipid molecules in biological cells, and nanoscale chemical imaging of single-wall carbon nanotubes (SWCNTs) in air and water (Step 41).

Alongside these three sections, we also describe the important process of analyzing TERS spectral and imaging data in order to obtain accurate and reliable information.

Advantages and limitations of TERS over existing techniques

A comparison of various alternative chemical imaging techniques is shown in Fig. 2, in which spatial resolution and chemical information content are used as figures of merit. Conventional vibrational and electronic spectroscopy techniques such as confocal Raman microscopy (CRM)[8,9], IR microscopy[10] and UV-visible[11] spectroscopy can provide chemical information, but are limited in sensitivity and spatial resolution. Although the sensitivity of Raman spectroscopy can be markedly improved using techniques such as SERS[12], resonance Raman spectroscopy[13] and stimulated Raman

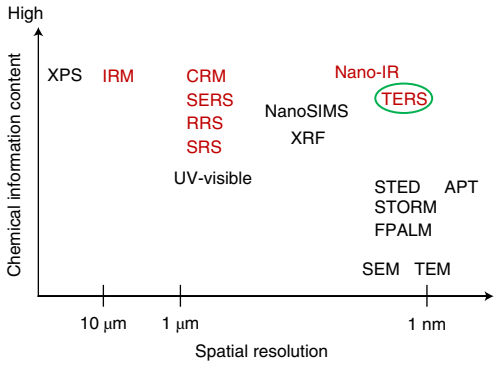

Fig. 2 | Comparison of TERS with other analytical techniques. A comparison of different chemical imaging techniques using spatial resolution and chemical information content as figures of merit. Techniques based on vibrational spectroscopy are highlighted in red for comparison. TERS has the potential to provide rich chemical information with very high spatial resolution. See Buurmans and Weckhuysen[100] for further discussion of other spatially resolved chemical characterization methods. APT, atom probe tomography; CRM, confocal Raman microscopy; FPALM, photo-activated localization microscopy; IRM, IR microscopy; RRS, resonance Raman spectroscopy; SEM, scanning electron microscopy; SRS, stimulated Raman spectroscopy; STED, stimulated emission depletion microscopy; STORM, stochastic optical reconstruction microscopy; TEM, transmission electron microscopy; XRF, X-ray fluorescence. Adapted with permission from Buurmans and Weckhuysen[29], Springer Nature.

spectroscopy[14], the spatial resolution remains diffraction limited to 200–300 nm. Nanoscale IR (Nano-IR) techniques such as scanning near-field IR microscopy and photo-induced force microscopy[15] have the potential for high-spatial-resolution chemical imaging[16], but strong IR absorption by water renders their application within aqueous and electrochemical environments challenging. Furthermore, the spatial resolution of Nano-IR imaging has typically been restricted to >10 nm[16], whereas TERS has been shown to provide chemical information with a spatial resolution approaching the molecular scale (<1 nm)[17].

The ability to visualize the nanoscale distribution of small biomolecules within biological cells is critical for probing sub-cellular biological nanostructures and molecular mechanisms of biological processes[18]. This requires non-destructive and label-free molecular mapping of biological cells at the nanoscale. The technique that is closest to fulfilling these criteria is super-resolution fluorescence microscopy (stimulated emission depletion microscopy, stochastic optical reconstruction microscopy and photo-activated localization microscopy)[19]. However, these techniques rely on the attachment of fluorophore labels to the molecules of interest, which may influence their chemical behavior.

Electron microscopy techniques such as scanning electron microscopy (SEM) and transmission electron microscopy can provide limited chemical information, but they typically require vacuum conditions. X-ray techniques such as X-ray photoelectron spectroscopy (XPS)[20] and X-ray fluorescence[21] are particularly powerful techniques that provide rich chemical information; however, these techniques have drawbacks as well. For example, XPS has a spatial resolution at a scale of tens of micrometers, in addition to the limitation of operation under vacuum. Operation of the these techniques at high spatial resolution and in ambient or liquid environments is feasible; however, such applications require highly specialized and expensive equipment, limiting their widespread application[22]. Similarly, nanoscale secondary ion mass spectrometry[23] and atom probe tomography[24] are also capable of providing valuable chemical information with high sensitivity and lateral resolution, but they are destructive in nature.

In contrast to the above-described techniques, TERS can be used for non-destructive investigation of samples in ambient as well as aqueous[25–29], organic liquid[30] and electrochemical[31–35] environments. TERS provides highly sensitive, spectral information at the nanoscale together with the surface topography, allowing a direct correlation of structural features with the surface chemistry. As a label-free technique, TERS can be used to study analyte molecules directly, particularly for the investigation of chemical composition and molecular dynamics in biological samples. Furthermore, metallic TERS probes can be also used to measure electrical signals, allowing the simultaneous collection of topographical, chemical and electrical information at the nanoscale[36,37]. Currently, such multi-parameter measurements cannot be obtained using any other analytical technique. Last, a plasmonically enhanced EM field can also enhance photoluminescence (PL) and fluorescence signals, allowing tip-enhanced photoluminesce[36,38,39] and tip-enhanced fluorescence[40,41] imaging at the nanoscale.

Although TERS offers numerous advantages for nanoscale chemical characterization, it does have limitations. Because TERS is an SPM-based technique, only relatively flat samples with a surface roughness of a few hundred nanometers can be successfully investigated. Furthermore, the penetration depth of TERS signals is typically <10 nm[36], such that only the very top surface of the sample can be analyzed. TERS provides information about only Raman-active molecules, placing a limitation on the range of systems that can be studied. Finally, quantitative chemical imaging has not yet been achieved, due to both uncertainties in molecular cross-sections associated with all molecular spectroscopies and the challenging aspects of variable signal enhancement factors of TERS probes. However, with continued research in this area by a growing community armed with the optimized procedures described in this protocol, we believe this technique will continue to develop, bringing new scientific insights into many different and exciting application areas.

TERS applications

Over the past two decades, TERS has been used to study a wide variety of samples in different disciplines of scientific research, providing valuable chemical insights. Being a label-free technique, TERS can be used to study molecules directly, investigating chemical composition and molecular dynamics in biological samples in particular. Therefore, TERS has been used in the life sciences to determine the chemical compositions of pathogens such as bacteria[42] and viruses[43], nucleic acids such as DNA[44] and RNA[45], lipid membranes[46], amino acids[47], peptides[48] and proteins[49–51], as well as to determine the distribution of small molecules within biological cells[52].

TERS has been equally effective in nanoscale chemical characterization of non-biological samples. For example, in 1D materials, TERS has been used to probe nanoscale variations in chirality, diameter, defects, strain and doping of carbon nanotubes[53–55], symmetry of the specific vibrational mode in GaN nanowires[56], diameter-dependent PL energy emissions in CdSe nanowires[57] and the fraction of crystalline and amorphous content in Ge nanowires[58]. Similarly, TERS has been effectively used to characterize defects, edges and contamination in single-layer graphene[59–61], and for studying excitonic processes at the nanoscale in single-layer transition metal dichalcogenides such as MoS_2[38,62], $MoSe_2$[63] and WSe_2[64]. More recently, TERS has been used for structural characterization of a new class of materials called covalent monolayers[65,66].

In addition to 1D and 2D materials, TERS has been used for in situ and ex situ characterization of different catalytic systems[13,67–72] and electrochemical processes[31,35]. TERS has been an impressive technique for correlating topography and chemical composition with local photocurrent generation in operational organic photovoltaic devices, providing valuable insights into the functioning mechanism[36,73]. Furthermore, TERS has been used for studying multilayer polymer thin films[74], interfaces of phase-separated domains in polymer-blend samples[75,76], local strain in semiconductors[77] and local phonon symmetry in crystalline materials[78]. Owing to its extremely high chemical sensitivity, TERS has been shown to be very effective in characterizing SAM of organic molecules[29,79–82] and has even been used to image individual *meso*-tetrakis(3,5-di-tertiarybutylphenyl)-porphyrin molecules with a spatial resolution of <1 nm, demonstrating the potential of TERS for the characterization of single molecules.

With a primary focus on nanoscale chemical imaging using TERS, this protocol is intended for researchers working in chemical, biological and material sciences where surface chemical characterization is required at nanometer scales.

Experimental design

Plasmonically active TERS probes

The success of TERS measurements critically depends on the quality of the TERS probes, because the EM field enhancement is highly sensitive to the radius and nanoscale morphology of the metal at the probe apex[4,83]. While the spatial resolution improves with decreasing probe radius, the field enhancement is strongly influenced by the nature of the sample. For a metallic probe in contact with a dielectric substrate (so-called 'non-gap mode'), the field enhancement has been shown to increase with decreasing probe radius[84]. By contrast, in the case of a metallic probe in contact with a metallic substrate ('gap mode'), the field enhancement increases when the probe radius is increased from 5–15 nm to 50–80 nm[85–87]. In our laboratory, we use Ag-coated TERS probes with a radius of ~25 nm for both gap and non-gap mode TERS measurements, which typically yield a spatial resolution on the order of 20 nm[60,68].

Although TERS probes are available commercially (e.g., from Horiba Scientific, NT-MDT, Bruker Nano, and Nanonics Imaging), they are more commonly prepared by in-house fabrication methods. However, production of plasmonically active probes with a high yield[88] is a challenge because of the general lack of detailed knowledge about optimized fabrication procedures. In addition, metal-coated TERS probes typically undergo rapid delamination and loss of plasmonic activity when exposed to a liquid environment[25]. Owing to this instability, TERS experiments in liquids have been mostly restricted to point spectroscopy measurements[25–28,31–35], and few investigations have attempted nanoscale 2D chemical imaging in a liquid environment using TERS[29,30]. Herein, we present a detailed step-by-step procedure to prepare highly active TERS probes suitable for chemical imaging in both air and liquids, with a yield approaching 100%[89]. We use this protocol to routinely prepare TERS probes for nanoscale chemical characterization of a range of different samples.

TERS system

TERS measurements can be achieved using either AFM or STM for positional feedback[1], and the excitation laser can be coupled with the TERS probe via a side or top-down illumination geometry or by illuminating the sample surface with the laser passing through the sample[1]. We use an AFM-based TERS system implemented in this latter transmission mode. This configuration allows TERS measurements to be implemented using a standard inverted confocal optical microscope in combination with an oil-immersion, high-numerical-aperture (high-NA) lens, providing a laser focal spot with minimized lateral dimensions and with high collection efficiency of the Raman-scattered light. Unlike STM-based TERS, which requires the sample to be electrically conductive, AFM-based TERS can be applied to both conductive and non-conductive substrates. However, because this type of illumination of the TERS probe requires laser transmission through the sample, this configuration is limited to optically transparent substrates.

Alignment of a TERS probe with the excitation laser

TERS probes must be correctly aligned with the excitation laser of the confocal Raman spectroscopy system for efficient excitation of the LSPR. This involves a number of steps, including positioning TERS probes at the center of the focal spot of the excitation laser while maintaining SPM feedback and locating the 'hotspot' at the TERS probe apex. This requires separate positioning systems for the TERS probe and the objective lens. Particular care must be taken in relation to aberrations in the laser beam and non-uniform distribution of laser intensity within the focal spot.

Nanoscale TERS imaging and data analysis

Successful TERS imaging requires a delicate balance between different experimental and acquisition parameters, including laser power, spectrum integration time and maintenance of the SPM feedback between the TERS probe and the sample surface. Furthermore, to confidently extract information from TERS data, correct procedures must be followed for data analysis and image processing, including peak fitting of the raw Raman spectra; these procedures are also discussed in this protocol.

Materials

Biological materials

- In the example described in this protocol (Step 41F), we use mouse preadipocytes (BioCat, cat. no. SP-L1-24-ZB), but the same approach can also be used with other biological samples, including pathogens such as bacteria and viruses, nucleic acids such as DNA and RNA, lipid membranes, amino acids, peptides, and proteins. **! CAUTION** Necessary health and safety approval must be obtained from the appropriate local authority before working with biological cells. The cell lines used in your research should be regularly checked to ensure that they are authentic and are not infected with mycoplasma.

Reagents

- Isopropyl alcohol (IPA, Sigma-Aldrich, cat. no. W292912-1KG-K)
- Ethanol (Sigma-Aldrich, cat. no. 34852-1L-M)
- Biphenyl thiol (BPT; Sigma-Aldrich, cat. no. 752207-1G)
- p-Aminothiophenol (pATP; 97% (wt/wt); Sigma-Aldrich, cat. no. 422967-25G)
- p-Nitrothiophenol (pNTP; Sigma-Aldrich, cat. no. N27209-5G)
- Poly(3,4-ethylenedioxythiophene):poly(styrenesulfonate) (PEDOT:PSS, aqueous solution, 1.3–1.7% (wt/vol) solid content; Heraeus Precious Metals, cat. no. CLEVIOS P VP AI 4083)

- Highly oriented pyrolytic graphite (HOPG; HQ Graphene, cat. no. Graphite HOPG ZYB)
- Sodium deoxycholate (>97% (wt/wt); Sigma-Aldrich, cat. no. D6750-10G)
- (3-Aminopropyl)triethoxysilane (APTES, 99% (wt/wt); Sigma-Aldrich, cat. no. 440140-100ML)
- N_2 gas (99.998%; BOC, cat. no. 19319561)
- Ar gas (99.998%; BOC, cat. no. 19319583 Rev 03)
- Epoxy resin (Agar Scientific, cat. no. AGR1031)
- Deuterated stearic-d_{35} acid (DSA, 99%; Sigma-Aldrich, cat. no. 448249-1G)
- Sodium hydroxide (99.99%; Sigma-Aldrich, cat. no. 306576-25G)
- PBS (pH 7.2–7.6; Sigma-Aldrich, cat. no. P5493-1L)
- 1,4-Piperazinediethanesulfonic acid (PIPES, pH 7.4; Sigma-Aldrich, cat. no. P1851-500G)
- 95% (wt/vol) Paraformaldehyde (Sigma-Aldrich, cat. no. 158127-100G)
- 8% (wt/vol) Glutaraldehyde solution (Sigma-Aldrich, cat. no. G7526)
- SWCNTs (National Institute of Standards and Technology, custom order) **! CAUTION** SWCNTs are nanomaterials and thus present a hazard that should be minimized per the guidelines at your institution or workplace, typically requiring local ventilation and appropriate personal protective equipment. For more information, see ref. [90].
- 2% (wt/vol) Osmium tetroxide (Sigma-Aldrich, cat. no. 75633) **! CAUTION** Osmium tetroxide is highly toxic upon inhalation, contact with skin or ingestion, and should be used only by trained scientists, in a fume hood, while wearing appropriate personal protective equipment.
- 30% (wt/wt) Hydrogen peroxide (Sigma-Aldrich, cat. no. H1009-100ML) **! CAUTION** Hydrogen peroxide is a highly toxic reagent. This reagent should be used in a fume hood while wearing appropriate personal protective equipment.
- Sulfuric acid (concentrated, 99.999% (wt/wt); Sigma-Aldrich, cat. no. 339741-500ML) **! CAUTION** Concentrated sulfuric acid is a highly toxic reagent. This reagent should be used in a fume hood while wearing appropriate personal protective equipment.

Metals

- Ag (Advent Research Materials, cat. no. AG548709) **▲ CRITICAL** The purity of Ag should be >99.99%. Lower purity will probably yield plasmonically inactive or contaminated TERS probes.
- Au (Advent Research Materials, cat. no. AU518007) **▲ CRITICAL** The purity of Au should be >99.99%. Lower purity will probably yield plasmonically inactive or contaminated TERS probes.
- Cr (Kurt J Lesker Company, cat. no. EVSCRW1)

Equipment

- Adhesive tape (Ultron Systems, cat. no. 1007R-6.0)
- Inverted confocal optical microscope (Nikon, model no. Eclipse Ti-U)
- Raman spectrometer (Horiba Scientific, cat. no. iHR 320)
- AFM (Horiba Scientific, CombiScope model)
- Electron-multiplying charge-coupled device (EMCCD; Andor Technology, Newton model)
- 532-nm Excitation laser (Coherent, model no. Compass 315M)
- 633-nm Excitation laser (Melles Griot, cat. no. 25-LHP-928-230)
- White-light LED source (CoolLED, cat. no. pE-100-WHT-20E-30)
- Oil immersion microscope objective (×100; Nikon, Apo TIRF model)
- Radial polarizer (ARCoptix, RPC model)
- Scanning electron microscope (Zeiss, model no. SUPRA 40)
- Vacuum thermal evaporation system (MBraun) with quartz crystal microbalance (Inficon)
- Purpose-built AFM probe holder for thermal evaporation system
- N_2 glovebox (MBraun, cat. no. MB 200B)
- Quartz tube furnace (Lenton Furnaces, cat. no. 4838)
- Heater (Electrothermal, cat. no. EM3000/CE)
- Purpose-built pre-humidifier **▲ CRITICAL** This equipment is optional and dry oxidation can be used as an alternative strategy for oxidation of Si AFM probes.
- UV-ozone chamber (UVOCS, cat. no. TIOXIO/OES/E)
- Contact-mode Si AFM probes (force constant: 0.18 N m^{-1}, resonance frequency: 13 kHz; MikroMasch, cat. no. HQ:CSC17/No Al-50)
- 13-mm Plastic coverslips in 24-well plates (Thermo Scientific, cat. no. 10252961)
- Ultramicrotome equipped with a diamond knife (Leica, cat. no. UC7)

- Water purification system (Merck Millipore, Milli-Q Integral model)
- Laser power meter (Thorlabs, cat. no. PM100D)
- Desiccator (Fisher Scientific, cat. no. 10528861)
- Ultrasonic bath (Fisher Scientific, cat. no. 11420998)
- UV–ozone cleaner
- Mo or W evaporation boats (Kurt J. Lesker, cat. no. EVSME3005MO or EVSME3005W)
- Spin coater (Laurell Technologies, cat. no. WS-650SZ-6NPP/LITE)
- Glass coverslips (thickness no. 1.5; Fisher Scientific, cat. no. 12392118) ▲ **CRITICAL** Ensure that the glass coverslips are cleaned thoroughly before using them for sample preparation. Coverslips can be cleaned by sonicating in IPA for 20 min, drying them using a flow of N_2 or Ar and finally placing them in a UV–ozone cleaner for 15 min. Allow the UV–ozone cleaner to cool for at least 15 min before removing the coverslips.

Software

- AIST-NT AFM software (Horiba Scientific, http://www.aist-nt.com/products/combiscopetm-1000)
- LabSpec 5 Raman spectroscopy software (Horiba Scientific, https://www.horiba.com/en_en/products/detail/action/show/Product/labspec-6-spectroscopy-suite-software-1843/)
- SPIP (Image Metrology, https://www.imagemet.com/products/spip/)
- OriginPro (Originlab, https://www.originlab.com/Origin)
- MATLAB software (MathWorks, https://www.mathworks.com/products/matlab.html)

Reagent setup

▲ **CRITICAL** All reagents in this section should be freshly prepared and used immediately after preparation.

Piranha-cleaned (3-aminopropyl)triethoxysilane-functionalized glass coverslips

1 Prepare 20 ml of piranha solution inside a fume hood by mixing 5 ml of hydrogen peroxide with 15 ml of concentrated sulfuric acid. ! **CAUTION** Preparation of piranha solution (sulfuric acid/hydrogen peroxide = 3:1 (vol/vol)) using sulfuric acid and hydrogen peroxide reagents must be performed in a fume hood. Piranha solution is an extremely strong oxidizing agent and should not be brought into contact with organic chemicals. It must be disposed of by neutralization and dilution with copious amounts of pure water.
2 Immerse the glass coverslips fully in the piranha solution.
3 Remove the coverslips from the piranha solution after 10 min, rinse them with copious amount of deionized water and blow-dry with a stream of nitrogen or argon gas.
4 To functionalize the piranha-cleaned glass coverslips with APTES, place them inside a sealed desiccator alongside 200 µl of APTES in an open vial for 12 h.

5 mM BPT in ethanol

Dissolve 4.7 mg of BPT in 5 ml of ethanol and sonicate for 10 min.

10 µM Deuterated stearate

1 Dissolve 3.2 mg of DSA in 1 ml of ethanol to prepare a 10 mM DSA stock solution.
2 Mix 1 ml of DSA stock solution with 500 ml of ethanol to prepare a 20 µM DSA solution.
3 Complex 50 ml of 20 µM DSA solution with 50 ml of 20 µM NaOH in ethanol to obtain 100 ml of 10 µM deuterated stearate solution.

4% (wt/vol) Paraformaldehyde and 1% (wt/vol) glutaraldehyde in 100 mM PIPES

Dissolve 4 g of paraformaldehyde and 3 g of PIPES in 87.5 ml of deionized water (resistivity at 25 °C: 18.2 MΩcm) and add 12.5 ml of 8% (wt/vol) glutaraldehyde solution in order to obtain 100 ml of 4% (wt/vol) paraformaldehyde and 1% (wt/vol) glutaraldehyde in 100 mM PIPES.

2.5% (wt/vol) Glutaraldehyde in 100 mM PIPES

Dissolve 3 g of PIPES in 70 ml of deionized water (resistivity at 25 °C: 18.2 MΩcm) and add 30 ml of 8% (wt/vol) glutaraldehyde solution to obtain a solution of 2.5% (wt/vol) glutaraldehyde in 100 mM PIPES.

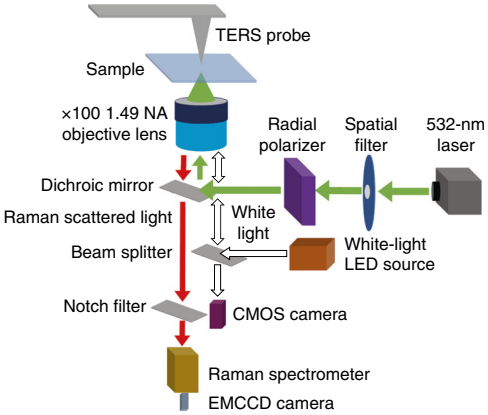

Fig. 3 | Optical configuration of the TERS system. A schematic diagram depicting the optical configuration of the transmission-mode AFM-TERS microscope in our laboratory. CMOS, complementary metal-oxide-semiconductor; EMCCD, electron-multiplying charge-coupled device; LED, light-emitting diode.

1% (wt/vol) Osmium tetroxide in 100 mM PIPES

Dissolve 3 g of PIPES in 50 ml of deionized water (resistivity at 25 °C: 18.2 MΩcm) and add 50 ml of 2% (wt/vol) osmium tetroxide solution to obtain a solution of 1% (wt/vol) osmium tetroxide in 100 mM PIPES.

Equipment setup

Oxidation apparatus

Coating an AFM cantilever with a material of lower refractive index such as SiO_2 or AlF_3 before Ag deposition has been shown to improve the yield and plasmonic signal enhancement of TERS probes[91–94]. Therefore, we decrease the refractive index of Si AFM cantilevers by introducing a thick oxide layer on the surface before metal deposition. Si AFM cantilevers can be oxidized using either a dry or wet oxidation process. Wet oxidation takes substantially less time (<1 h) compared to dry oxidation (>10 h) to obtain an SiO_2 thickness of ~300 nm. Therefore, we use a purpose-built wet oxidation apparatus consisting of a quartz tube furnace, which is fed by air passing through a pre-humidifier consisting of a sealed water bath placed on a heater. Si AFM probes are placed in the center of the tube furnace and exposed to a flow of steam from the pre-saturator.

Vacuum thermal evaporator

The deposition of metals (Cr, Au and Ag) onto the probe apex of an oxidized AFM cantilever to create a TERS probe can be carried out using different physical vapor deposition techniques such as thermal evaporation, e-beam evaporation or sputtering[95]. We carry out the metal deposition inside a vacuum thermal evaporation system, which is placed within an N_2 glovebox with an oxygen and moisture concentration of <0.1 p.p.m. Placing the evaporation apparatus inside an N_2 glovebox keeps it free from the organic contamination present in the ambient environment. Furthermore, the freshly prepared TERS probes can be immediately stored in the glovebox for up to 5 months without substantial loss of their plasmonic signal enhancement capability[89].

TERS system

We use a bespoke transmission-mode TERS system consisting of an AFM secured to the top of an inverted confocal optical microscope attached to a Raman spectrometer and an EMCCD detector. A schematic diagram of the optical configuration of our TERS system is presented in Fig. 3. A 532-nm excitation laser is focused on the sample using a 1.49 NA, ×100 oil immersion microscope objective. Intensity aberrations in the laser beam path are removed using a purpose-built spatial filter (pinhole: 10 μm). To fully illuminate the objective lens aperture, the laser beam diameter is expanded to 10 mm using a plano-convex lens. A high z-component of the electric field in the laser focal spot is achieved by passing the expanded laser beam through a radial polarizer. A white-light LED source (Fig. 3) is used to illuminate the sample for co-localization of the probe with the area of interest. All TERS measurements are performed using contact-mode AFM feedback. Far-field measurements are conducted by retracting the TERS probe from the sample and refocusing the laser at the same spot on the

sample. TERS data are acquired using dedicated TERS software, which is a combination of the AIST-NT AFM software and LabSpec 5 Raman spectroscopy software. Data analysis is carried out using SPIP, LabSpec 5, OriginPro and MATLAB software.

Procedure

Preparation of TERS probes ● Timing 22.5 h

▲ **CRITICAL** The first stage in performing TERS measurements is the preparation of robust plasmonically active TERS probes, which is described in Steps 1–8. Before using TERS probes for measurements, it is important to ensure that they are of sufficient quality. This is done using Steps 9–11.

1 *Oxidation of Si AFM probes (Steps 1–3)*. Place Si contact-mode AFM cantilevers with no metal back-coating into the middle of a tube furnace. Set the temperature of the tube furnace to 1,000 °C.

2 Once the required temperature is reached, introduce steam into the furnace via continuous passage of the feed gas through a heated water pre-saturator for 45 min.

▲ **CRITICAL STEP** The thickness of the oxide layer produced on the Si cantilevers depends on the temperature of the furnace and time of exposure to the steam. Once the flow of steam is stopped, the oxidation of the Si surface becomes extremely slow. Ensure that the oxidized cantilevers have a purple or green surface coloration, which indicates an oxide layer thickness of >300 nm. Oxidation of Si cantilevers can also be achieved without using steam. In this case, the Si cantilevers should be placed in a furnace at 1,000 °C for 10 h in order to achieve the required oxide thickness.

3 Allow the tube furnace to cool to room temperature (20–25 °C) for 14 h.

▲ **CRITICAL STEP** Do not remove the cantilevers from the furnace until it has cooled to room temperature.

4 *Cleaning of oxidized AFM probes (Step 4)*. Remove the oxidized cantilevers from the furnace and place them inside a UV–ozone cleaner for 1 h to remove any organic contamination from the surface. Allow 30 min for the UV–ozone chamber to cool and the ozone to decompose before removing the AFM cantilevers.

▲ **CRITICAL STEP** Upon exposure to the ambient environment, the surface of the oxidized AFM cantilevers is typically contaminated by a layer of organic material. If the cantilevers are not cleaned before the deposition of Ag, a strong signal from organic molecules may be observed in the TERS measurements, obscuring the TERS signal from the sample. Furthermore, this contaminant layer may also affect the strength of Ag adhesion to the surface, thus reducing the durability of the TERS probes.

5 *Metal deposition (Steps 5–8)*. Clean the Cr, Au and Ag source materials through ultrasonication in IPA for 20 min and drying with an inert (N_2 or Ar) pressurized gas. Place cleaned Cr, Au and Ag materials into three different Mo or W evaporation boats inside the thermal evaporator.

▲ **CRITICAL STEP** For performing TERS measurements in a liquid environment, it is essential to use a multilayer metal coating to prepare the TERS probes in order to maximize the adhesion of Ag to the AFM probe apex. In our recently published study, we found that Cr alone does not improve the adhesion of Ag to the oxidized Si AFM probes sufficiently to allow TERS measurements in liquids[29]. A buffer layer of Au is required to achieve strong adhesion. The water resistance of the multilayer metal-coated probes probably arises from an improvement in the continuity of the Ag film. For TERS measurements in environments other than liquid (air or ultrahigh vacuum), a metal coating of only Ag would suffice.

6 Clean the purpose-built probe holder for the thermal evaporator by rinsing in IPA and drying with an inert (N_2 or Ar) pressurized gas. Mount the oxidized and cleaned cantilevers onto the probe holder and place in the evaporator at a distance of ~20 cm above the evaporation sources. Pump down the evaporation chamber until a pressure of $\leq 10^{-6}$ mbar is achieved.

▲ **CRITICAL STEP** To prepare contamination-free TERS probes, the evaporator must be kept free from organic contaminants, which can lead to unreliable results. Organic contamination of the evaporator can be reduced by heating an empty evaporation boat at ~960 °C for 12 h at a pressure of $\leq 10^{-6}$ mbar. If this step is performed, the evaporator must be left to cool for 24 h before any preparation of TERS probes.

7 Slowly increase the temperature of the Cr evaporation source until an evaporation rate of 20 pm s^{-1} is reached, as measured using a calibrated quartz crystal microbalance. Deposit a 3-nm-thick Cr film on the TERS probes. Next, deposit a 10-nm-thick Au film on the TERS probes at an evaporation rate of 30 pm s^{-1}. Finally, deposit a 100-nm-thick Ag film on the TERS probes at an evaporation rate of 50 pm s^{-1}.

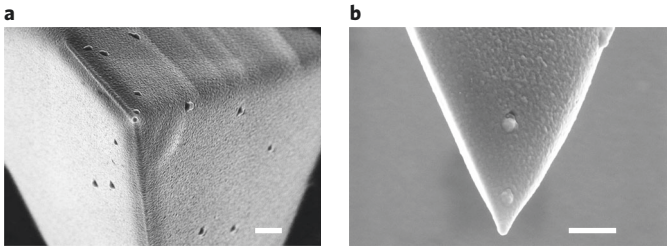

Fig. 4 | Inspecting the quality of TERS probes using SEM imaging. a,**b**, SEM image of a representative Cr-, Au- and Ag-coated TERS probe measured from above (**a**) and the side (**b**). Scale bars, 500 nm. The dark features visible in **a** represent irregular protrusions in the probe coating, two of which are more clearly visible in the side view of the probe (**b**). Note that the size of the grains in the Ag film is in the order of a few tens of nanometers[89], which is essential for excitation of a strong localized surface plasmon resonance (LSPR) with the 532-nm excitation laser.

▲ **CRITICAL STEP** The deposition of Cr and Au must be carried out without breaking the vacuum. It is also desirable, although not essential, that the Ag be deposited without breaking the vacuum.

▲ **CRITICAL STEP** For TERS measurements in environments other than liquid (air or ultrahigh vacuum), a metal coating of only Ag would suffice. Therefore, in this case, directly perform deposition of 100-nm-thick Ag film onto oxidized Si AFM probes, excluding the steps of Cr and Au deposition.

8 Allow the evaporation chamber to cool for at least 4 h before removing the TERS probes from the evaporator.

■ **PAUSE POINT** The TERS probes can be stored in a N_2 or Ar atmosphere until they are required for measurements. TERS probes can be stored up to 5 months inside a N_2 or Ar glovebox at room temperature with an O_2 and H_2O concentration of <0.1 p.p.m. without a substantial loss of plasmonic sensitivity. If stored in a vacuum desiccator, TERS probes should be used within 3 d of preparation. For best results, TERS probes should be prepared on the same day they are required, in order to minimize both oxidation and contamination of the Ag coating.

9 *TERS probe quality check (Steps 9–11).* From each batch of freshly prepared TERS probes, select one probe at random for SEM imaging.

▲ **CRITICAL STEP** The quality of a particular batch of TERS probes can be assessed by performing SEM imaging of one probe selected at random from the batch. If the quality of the selected probes is acceptable, as described below, the other probes in the batch can then be used for TERS imaging.

10 Place the probe on the SEM sample holder with the probe apex facing upward. Perform SEM imaging of the probe apex from above.

? TROUBLESHOOTING

11 Now angle the TERS probe at ~45° and perform SEM imaging of the side of the probe. Example SEM images of a representative TERS probe are shown in Fig. 4.

▲ **CRITICAL STEP** If the probe shows an apex size of ≈50 nm and a continuous film of Ag at and around the probe apex, it is suitable for TERS measurements. Otherwise, the metal deposition procedure should be optimized until a continuous Ag film is achieved.

Preparation of the TERS system ● Timing 5 h

▲ **CRITICAL** Before performing TERS measurements, an excitation laser focal spot close to the diffraction-limited size should be obtained on the sample, as described in Steps 12–17. Furthermore, the TERS probe must be properly aligned with the excitation laser (Steps 19–33), and the near-field (EM-enhanced region) hotspot needs to be located at the probe apex (Steps 34–40) before performing TERS imaging (Step 41).

12 *Laser alignment of the Raman microscope (Steps 12–17).* First determine the diffraction-limited spatial resolution of the Raman microscope. This can be calculated from the wavelength (λ) of the excitation laser and NA of the objective lens, using Abbe's equation[96]:

$$\text{Abbe resolution}_{x,y} = \frac{\lambda}{2\text{NA}}. \quad (1)$$

13 Switch on the excitation laser and allow it to warm up according to the manufacturer's specifications. Pass the excitation laser of the Raman microscope through a spatial filter to remove

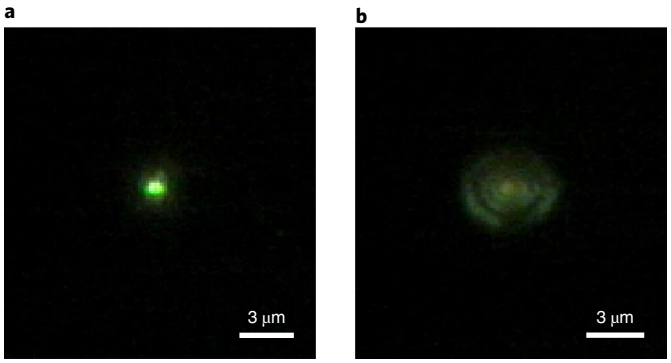

Fig. 5 | Diffraction-limited focal spot of the excitation laser. a, Optical image of the focal spot of a 532-nm excitation laser on a glass substrate. **b**, Optical image of a slightly defocused laser spot, demonstrating the airy pattern expected for a diffraction-limited spot.

any intensity variations in the beam and expand the beam diameter to the size of the back aperture of the objective lens. Pass the expanded and collimated beam from the spatial filter through a radial polarizer as depicted in Fig. 3. To achieve the smallest focal spot on the sample, align the optical path so that the laser beam enters the center of the objective lens of the confocal Raman microscope. To do this, mount an optical tube fitted with an alignment target in place of the objective lens. Ensure that the laser beam passes through the center of the alignment target. Then secure the objective lens onto the microscope.

▲ **CRITICAL STEP** To obtain a diffraction-limited focal spot at the sample, the laser beam must be collimated and its diameter should be similar to the size of the back aperture of the objective lens. This is achieved with the spatial filter in the optical path of the laser beam. Furthermore, for high enhancement of the EM field intensity at the TERS probe apex, the electric field of the excitation laser must be aligned in the *z*-direction within the focal spot, which can be best achieved using a radial polarizer in combination with a high-NA objective lens.

14 Clean the oil immersion objective lens, using IPA and a lens cleaning tissue in one sweeping motion to avoid scratching the lens surface. Place a laser power meter in the sample position and adjust the output power of the laser system so the power measured at the objective lens is <1 mW. Apply fresh oil to the objective lens using an oil dropper.

15 Place a glass coverslip in the sample position and add a small amount of oil to the top of the coverslip. Secure a Si wafer on top of the coverslip, with the front (polished) side facing downward. Allow 20 min for the oil to settle before checking the diffraction-limited focal spot in the optical view of the TERS microscope.

▲ **CRITICAL STEP** A diffraction-limited focal spot at the sample surface must have a tight circular shape, as shown in Fig. 5a. Furthermore, upon slightly changing the microscope focus, circular rings with an airy pattern must be visible in the focal spot (Fig. 5b). If neither a circular shape nor an airy pattern is observed in the focal spot, realign the optical path of the excitation laser beam from Step 13.

16 Check the calibration of the Raman spectrometer. Ensure that a Rayleigh scattering line at 0 cm^{-1} and the first-order Si Raman band positioned at 520 cm^{-1} are observed in the Raman spectra.

17 Maximize the intensity of the Si Raman band by adjusting the focus of the laser beam using the microscope focus and aligning the position of the confocal pinhole of the multimode fiber collecting Raman scattered light. The intensity of this peak and the acquisition parameters should be recorded to allow comparisons during other measurements so the performance of the system can be monitored over time.

18 *Laser alignment quality check (Steps 18–21).* An estimate of the focal spot size can be obtained by confocal Raman imaging of a SWCNT. Prepare a SWCNT substrate by drop-casting a liquid dispersion of SWCNTs on a glass coverslip. For the best results, deposit SWCNTs from a solution of 1% (wt/vol) deoxycholate (DOC) onto piranha-cleaned APTES-functionalized glass coverslips (Reagent setup).

19 Locate a suitable region of SWCNTs by confocal Raman imaging of a 50 × 50-μm region of the sample with a pixel size of 1 μm and integration time of 1 s. Perform high-resolution confocal Raman imaging of an isolated SWCNT, using a maximum step size of 20 nm.

Box 1 | Processing of TERS spectral and imaging data ● Timing 1–2 h

The following procedure should be adopted for the analysis of TERS spectra and images.

Procedure

1 If the Raman band of interest in the TERS spectrum is well isolated (such as the 2D band of single-layer graphene[61] or the G band of SWCNTs), extract the spectral region containing the Raman band. Fit the Raman band with a Lorentzian curve after linear background subtraction of the extracted spectral region. Use the height of the fitted Lorentzian curve as the intensity of that particular TERS band.
▲ **CRITICAL STEP** Consider only the TERS spectra with a peak intensity to background noise ratio (S/N ratio) of at least 3:1 for data analysis.
▲ **CRITICAL STEP** If the Raman band of interest in the TERS spectrum overlaps other bands or contains several bands in close proximity, then extract the entire spectral region containing all Raman bands. Fit all Raman bands in the extracted region with Lorentzian curves after linear background subtraction and use the fitted heights as the intensities of the particular TERS bands.

2 Determine the enhancement factor (EF) of a Raman band in the TERS spectrum. The EF is defined as:[74]

$$EF = \left(\frac{I_{TERS}}{I_{FF}} - 1\right)\frac{V_{FF}}{V_{NF}}, \quad (3)$$

where, V_{NF} and V_{FF} are the sampling volumes associated with the near-field and far-field measurements, respectively. In general, it is not possible to accurately determine the 3D distribution of the near field generated by a TERS probe. However, in the case of single-layer 2D materials, such as graphene[60] and single-layer MoS_2 (ref. [38]), the near-field and far-field sampling volumes in Eq. (3) can be approximated by the respective near-field (A_{NF}) and far-field (A_{FF}) probe areas at the sample surface. Estimate these probe areas from the diameter of the TERS probe apex measured using SEM imaging and the diameter of the excitation laser focal spot, respectively. Note that the uncertainty of the value of A_{NF} may still be large using this method; however, the EF of a TERS band can be calculated using the following equation[25,74]

$$\mathrm{EF} \approx \left(\frac{I_{\mathrm{TERS}}}{I_{\mathrm{FF}}} - 1\right)\frac{A_{\mathrm{FF}}}{A_{\mathrm{NF}}}. \quad (4)$$

▲ **CRITICAL STEP** When the number of molecules present within the probe volume of the excitation laser spot is very small, for example, in the case of a molecular SAM on a metal substrate such as Au[81], generally no Raman signal is observed in the far field. However, in the TERS spectrum, the Raman bands become visible due to the strong plasmonic enhancement of the electric field in the nanoscale gap between the two metal surfaces. For such samples, it is not possible to obtain an accurate estimate of the EF. However, a minimum value of the EF can be obtained using Eq. (4), assuming that the intensity of the far-field Raman signal is at least equal to the noise level in the far-field spectrum[29]. In this case, estimate I_{FF} in Eq. (4) from the noise level in the far-field spectrum, which is calculated from the standard deviation of the Raman intensity in the same spectral region as the TERS band.

3 To generate a TERS image, analyze each spectrum at each pixel, using steps 1 and 2. Use the height of the fitted Lorentzian curve at each pixel to generate a 2D image of the TERS band of interest.

4 A TERS image represents a convolution of both the near field at the TERS probe apex and the far field of the excitation laser with the spatial dimensions of the features present on the sample. Therefore, an accurate calculation of the spatial resolution requires analyzing the TERS response across an infinitely small sample feature. In practice, the spatial resolution can be estimated only by choosing the sharpest regions of spectral contrast in the TERS image that correspond to realistic surface features, so that this convolution is minimized (for the most accurate estimate of spatial resolution, 1D structures such as carbon nanotubes are the most suitable samples). For each feature to be analyzed, extract a TERS intensity line profile and fit the data with two Gaussian curves to separate the near-field and far-field contributions. Estimate the spatial resolution of the TERS image from the FWHM of the Gaussian curve corresponding to the near-field contribution[101], as illustrated in Fig. 8 using the TERS image of a SWCNT.

20 Perform Lorentzian fitting of the 1,591-cm^{-1} band (G band) after linear background subtraction as described in Box 1. Generate a 2D image, using the intensity of the fitted 1,591-cm^{-1} band.

21 Extract three line profiles from perpendicularly across the SWCNT and fit the cross-section data to a Gaussian curve. For a diffraction-limited focal spot, the average of the full-width at half maximum of the fitted Gaussian curves should be close to the value obtained from Eq. (1) in Step 12, as shown in Fig. 6.
▲ **CRITICAL STEP** If the experimentally determined value of the confocal Raman spatial resolution is substantially larger (greater than 2×) than the theoretical value obtained from Eq. (1), recheck the alignment and quality of the laser beam.

22 *Alignment of the TERS probe with the excitation laser (Steps 22–33).* Remove the SWCNT sample and replace it with the sample under investigation.

23 Mount a TERS probe onto the AFM probe holder and then fit the AFM probe holder onto the AFM apparatus.

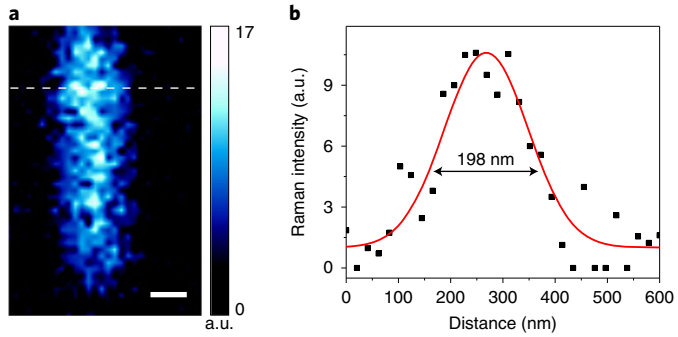

Fig. 6 | Estimating the far-field spatial resolution of a TERS system via Raman imaging of an SWCNT. a, Confocal Raman image generated from the 1,591-cm^{-1} band of an isolated SWCNT. Pixel size: 20 nm; integration time: 1 s. Scale bar, 100 nm. **b**, Intensity profile along the line marked in **a** fitted with a Gaussian curve (red line) after linear background subtraction, which is close to the Abbe's diffraction-limited spatial resolution of 178.5 nm of our Raman microscope, calculated using Eq. (1). SWCNT, single-wall carbon nanotube.

24 Align the AFM laser used to measure the cantilever deflection with the back of TERS probe cantilever and optimize reflection onto the photodiode by adjusting its position according to the AFM manufacturer's instructions. Position the probe in the correct lateral position relative to the sample area under investigation, with the TERS probe a few millimeters away from the sample surface.

25 Align the apex of the TERS probe roughly with the white-light focal spot on the sample via visual inspection of the apparatus.

26 Mark the position of the excitation laser focal spot in the optical view window of the TERS software.

27 Move the TERS probe toward the sample surface. Stop the approach as soon as the cantilever appears in the optical view of the TERS software. Ensure that the cantilever is stopped at least 10 μm away from the sample surface.

▲ **CRITICAL STEP** Ensure that the probe approaches the sample surface at a very slow speed and that it is stopped before making contact with the sample surface.

28 Move the TERS probe laterally until the cantilever is visible in the optical view window of the TERS software.

29 Once the TERS cantilever appears in the optical view, move the probe apex to the marked position of the laser spot, using the coarse positioning stepper motor for the TERS probe holder.

30 Move the TERS probe toward the sample surface, using the AFM feedback mechanism. Use suitable approach parameters to minimize the force of the contact between the TERS probe and the surface in order to preserve the structural integrity of the metal coating.

▲ **CRITICAL STEP** If the TERS probe comes into contact with the sample surface with a large amount of force, it will damage the metal coating of the probe, rendering it unsuitable for TERS measurements. The approach speed and the feedback gain parameters must be optimized to ensure that the metal coating at the TERS probe apex remains intact.

31 After the TERS probe has made contact with the sample surface, confirm that the cantilever deflection is stable and thus the AFM contact-mode feedback is operating correctly. Determine the optimum deflection set point for reliable feedback, which minimizes the force applied to the sample by the TERS probe, by reducing the deflection set point until the feedback becomes unstable and then increasing the deflection set point until the cantilever deflection is stable again. The feedback gain should also be optimized by increasing the gain until uniform oscillations are observed and then decreasing the gain so the oscillations disappear.

32 Locate the position of the TERS probe apex on the sample surface optically by adjusting the optical microscope focus.

33 Laterally position the objective lens, using the fine-positioning piezo scanner of the objective lens so that the TERS probe apex is aligned with the marked laser focal spot.

▲ **CRITICAL STEP** After the TERS probe is in contact with the sample, any movement of the sample or the objective lens must be carried out using the piezo scanner. Furthermore, the sample or the objective lens should be moved in small steps of <2 μm to avoid exerting large forces at the probe apex, which could lead to the loss of AFM feedback and/or damage to the metal coating of the probe apex.

34 *Location of near-field hotspot at TERS probe apex (Steps 34–38).* Measure a Raman spectrum for the sample under investigation with an integration time of 1s and calculate the ratio of

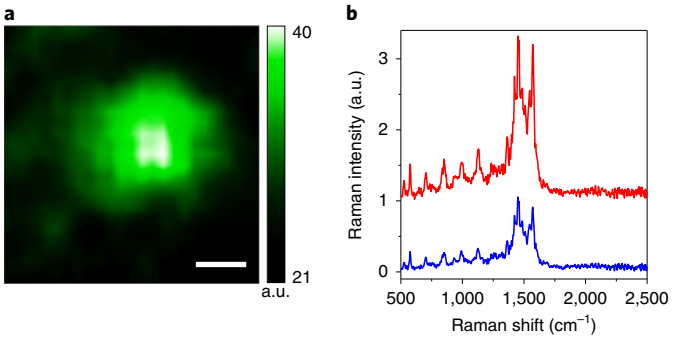

Fig. 7 | Assessing the sensitivity of a TERS probe via near-field hotspot imaging. a, Raman intensity image around a TERS probe apex in contact with a PEDOT:PSS thin film sample. The image was generated from the total intensity in the 1,230–1,720-cm^{-1} region of the PEDOT Raman spectra. Pixel size: 20 nm; integration time: 1 s. Scale bar, 100 nm. **b**, Raman spectra measured at the location of highest signal intensity in **a** (red) and 1 μm away from it (blue). Integration time: 30 s. In this case, the intensity of the 1,454-cm^{-1} PEDOT Raman band has a contrast of 1.2 at the center of the TERS hotspot.

the peak intensity for the most intense Raman band characteristic of the material versus the peak-to-peak value of the noise of the background signal, denoted herein as the S/N ratio. Decrease the laser power until the S/N ratio is ~5. The maximum laser power at the sample should be <300 μW.

▲ **CRITICAL STEP** The quality of a TERS image directly depends on the S/N ratio of the TERS spectra. Although the S/N ratio may be improved by using a high laser power, this increases the risk of thermal damage to the sample due to high temperature generated in the near field. Therefore, the minimum laser power providing a S/N ratio of at least 5 within a spectrum integration time of 1 s should be used for TERS measurements.

35 While the TERS probe and the sample are stationary, perform Raman imaging of a 1 × 1-μm area including the TERS probe by moving the objective lens in a raster fashion, using the appropriate piezo scanner. Use a step size of between 50 and 100 nm, while measuring a Raman spectrum at each pixel. Ensure that the AFM feedback is maintained while acquiring the image.

36 Generate a Raman image, using the intensity of a Raman band from the sample (see example hotspot image shown in Fig. 7a for PEDOT:PSS thin film sample).

37 Position the excitation laser beam at the point of maximum Raman intensity, i.e., the hotspot, by slowly moving the objective lens laterally, using the piezo scanner.

▲ **CRITICAL STEP** If no TERS hotspot is observed, replace the TERS probe with a new one and repeat Steps 23–37.

? TROUBLESHOOTING

38 Acquire a higher-resolution Raman image of a 500 × 500-nm area around the point of maximum Raman intensity by moving the objective lens with a step size of 20 nm and repeating Steps 36 and 37.

▲ **CRITICAL STEP** If the sample does not contain a uniform distribution, or a sufficient concentration, of analyte molecules on its surface, the PL intensity of the Ag coating (spectral range: 100–250 cm^{-1}) can be used instead to locate the hotspot by following Steps 35–38.

? TROUBLESHOOTING

39 *Near-field hotspot quality check (Steps 39 and 40).* For samples covering the entire substrate uniformly, such as polymer thin film samples[89], measure the Raman signal at the TERS hotspot and 1 μm away (laterally) from the hotspot, as shown in Fig. 7b.

▲ **CRITICAL STEP** For samples covering the substrate non-uniformly, or where the far-field Raman signal intensity of the sample is too weak, we recommend performing hotspot mapping using the PL intensity of the Ag coating. To do this, calculate the ratio of the PL signal measured at the hotspot to the substrate signal 1 μm away from the hotspot. Ensure that a minimum contrast (Eq. (2)) of 1 is obtained before using the probe for TERS measurements. If this strategy is used, proceed directly to Step 41.

40 Using the formula in Eq. (2), calculate the contrast[74] by comparing the near-field intensity of the Raman band under investigation with the intensity of the same peak determined from the far-field Raman spectrum 1 μm away (as shown in Fig. 7b):

$$\text{Contrast} = \frac{I_{\text{TERS}}}{I_{\text{FF}}} - 1, \quad (2)$$

where, I_{TERS} and I_{FF} are the Raman intensity of the peak measured at the TERS hotspot and in the far field, respectively. The far-field Raman spectrum must be measured using the same integration time and laser power as used to measure the TERS spectrum at the hotspot. If a contrast of ≥1 is achieved, the probe is sufficiently sensitive for TERS imaging.

▲ **CRITICAL STEP** Contrast provides an indication of the likelihood of success of a TERS imaging experiment. A high contrast value implies a strong plasmonic enhancement at the TERS probe apex, which is more likely to provide a high-resolution TERS image. If a contrast of <1 is obtained, the TERS probe should be realigned with the excitation laser, by following Steps 24–33, and the TERS hotspot should be located again by following Steps 34–38. If a suitable contrast value is still not achieved, a new TERS probe should be used, and the protocol should be followed from Step 23.

▲ **CRITICAL STEP** Plasmonic enhancement of Raman signals depends on the sample characteristics and varies from sample to sample. However, the probe should be used for TERS measurements only if a minimum contrast of 1 is obtained.

Experimental procedures for nanoscale imaging using TERS

41 In this section, we present seven experimental procedures for performing nanoscale chemical imaging using TERS on different samples. For TERS imaging of a single-layer graphene sample[60], follow option A. For TERS measurement of a PEDOT:PSS thin film on glass[74], follow option B. For TERS measurement of a SAM of BPT on Au[29], follow option C. For monitoring of the pNTP → 4,4′-dimercaptoazobenzene (DMAB) photocatalytic process using TERS[67], follow option D. For nanoscale imaging of the pATP → DMAB photocatalytic reaction using TERS[68], follow option E. For imaging of newly synthesized phospholipid (NSP) molecules in biological cells using TERS[52], follow option F. For nanoscale chemical imaging of SWCNTs in air and water using TERS[29], follow option G.

(A) **Performing TERS imaging of a single-layer graphene sample** ● **Timing 8 h**

(i) Prepare a single-layer graphene sample on a clean glass substrate, using mechanical exfoliation, in which graphite is cleaved by use of adhesive tape and this same tape is subsequently used to deposit graphene and graphite flakes onto a substrate[59].

(ii) Use confocal Raman imaging to identify a single-layer graphene flake on the sample[60]. Approach the identified graphene layer with the TERS probe until it generates contact-mode AFM feedback, using the approach parameters determined in Steps 23–33 to minimize the force on (and therefore the damage to) the TERS probe. Position the TERS probe apex in the center of the graphene flake and use the Raman intensity of the G band (~1,580 cm^{-1}) to locate the TERS hotspot by following Steps 34–38.

▲ **CRITICAL STEP** To locate the TERS hotspot accurately, it is important to place the TERS probe apex in the central region of the graphene flake (i.e., away from the edge of the flake). However, if the size of the graphene flake is only a few hundred nanometers, it may be difficult to position the TERS probe apex at the center of the flake. In this case, land the TERS probe on the glass substrate near the graphene flake and locate the TERS hotspot by following Steps 35–38, using the PL intensity of the Ag coating.

(iii) Measure the spectrum at the location of the TERS hotspot and determine the Raman intensity of the G band. Using Eq. (2), calculate the contrast by comparing the intensity of G band determined from the TERS hotspot and the far-field Raman spectrum measured before moving the TERS probe toward the surface. The far-field Raman spectrum must be measured using the same integration time and laser power as those used to measure the TERS spectrum at the hotspot. If a graphene G band contrast of ≥1 is achieved, the probe is sufficiently sensitive for TERS imaging.

(iv) Once the TERS hotspot has been successfully located, set the area of the TERS image to 2 × 2 μm. Set the pixel size to 40 nm, the spectrum integration time to 1 s, and the wavenumber range to 300–3,000 cm^{-1}.

(v) Set the software to record the topography, lateral force, and deflection (i.e., feedback signal) AFM data, as well as the Raman spectra at each pixel.

(vi) From the 2 × 2-μm TERS image, choose the area of interest and repeat step (iv) and (v), but instead use a step size of 10 nm for a region of 500 × 500 nm.

▲ **CRITICAL STEP** The spatial resolution of a TERS map depends on the size of the near-field region at the TERS probe apex, which could be substantially smaller than the apex size. Therefore, to obtain the highest-resolution TERS image, the smallest step size should

be used. However, a smaller step size increases the total number of pixels measured in the image, thereby increasing the total imaging time. Over longer periods (>3 h) of imaging, the alignment of the TERS probe to the excitation laser can be compromised due to thermal drift, leading to a loss of TERS signal enhancement. Therefore, for best results, restrict the total measurement time of the TERS image to <2 h.

? TROUBLESHOOTING

(vii) Generate TERS images of the 2D, D and G graphene Raman bands with the fitted band intensities at ~2,680 cm^{-1}, 1,340 cm^{-1} and 1,580 cm^{-1}, respectively, as described in Box 1.

(viii) When a TERS image shows areas of scientific interest, repeat the TERS imaging procedure in step (vi) to ensure measurement repeatability.

(ix) When a reduction in the lateral resolution is observed in the TERS image, realign the TERS probe with the excitation laser spot, following the hotspot location procedure outlined in Steps 34–38. If the hotspot is not of a size similar to its original measurements, or several hotspots are found, then the Ag coating at the probe apex may have been damaged. In this case, replace the TERS probe, following the protocol from Step 23.

(x) After the TERS measurements, check the cleanliness of the TERS probe by measuring the Raman spectrum at the TERS probe apex. To do this, replace the graphene sample on the TERS microscope with a clean glass coverslip, locate the hotspot by following Steps 23–38, and measure the Raman spectrum at the hotspot. If the sample signal is observed in the spectrum, then the TERS probe is contaminated with the sample. In this case, the results of the TERS imaging obtained using the contaminated probe are not reliable, and the TERS imaging should be repeated with a fresh TERS probe.

(xi) Process the TERS spectral data as described in Box 1.

(B) **TERS measurement of a PEDOT:PSS thin film on glass ● Timing 2 h**

(i) Clean a glass coverslip by sonicating it in IPA for 20 min, drying it using a flow of N_2 or Ar, and finally placing it in a UV–ozone cleaner for 15 min. Allow the UV–ozone cleaner to cool for at least 15 min before removing the coverslip.

(ii) Spin-coat 60 µl of aqueous solution of PEDOT:PSS onto a clean glass coverslip at 2,000 r.p.m. for 2 min in an Ar or N_2 environment.

(iii) Following Steps 22–33, load the sample into the TERS instrument and approach the surface with the TERS probe until it generates contact-mode AFM feedback, using the previously determined approach parameters in Steps 23–33 to minimize the force on (and therefore the damage to) the TERS probe. Use the procedure described in Steps 34–38 to perform confocal Raman imaging around the probe apex in a 2 × 2-µm area, using a pixel size of 80 nm, integration time of 1 s, and laser power (at the sample) of ~100 µW.

(iv) Create a near-field hotspot map, using the intensity of the 1,454-cm^{-1} (symmetric stretch of C=C bond in thiophene unit, $\nu_{sym\ C\alpha=C\beta}$) PEDOT Raman band.

(v) Select an area of 500 × 500 nm around the hotspot. Perform confocal Raman imaging around the hotspot, using a pixel size of 20 nm and integration time of 1 s. Create a new hotspot map, using the 1,454-cm^{-1} band intensity.

(vi) Measure a TERS spectrum at the position of the new hotspot, using an integration time of 10 s.

(vii) Retract the TERS probe. Refocus the laser at the same position on the sample and measure a far-field spectrum with an integration time of 10 s.

(viii) Process the TERS spectral data as described in Box 1.

(ix) Calculate the TERS contrast of the 1,454-cm^{-1} PEDOT Raman band, using Eq. (2).

(C) **TERS measurement of a SAM of BPT on Au ● Timing 6 h**

(i) Clean a glass coverslip by sonicating it in IPA for 20 min, drying it using a flow of N_2 or Ar and finally placing it in a UV–ozone cleaner for 15 min. Allow the UV–ozone cleaner to cool for at least 15 min before removing the coverslip.

(ii) Deposit 3 nm of Cr, followed by a 10-nm Au layer, on the clean glass coverslip via thermal evaporation, using the same process as described in Steps 5–8 for coating the TERS probes.

(iii) Immerse the Cr–Au-coated coverslip in a 5 mM solution of BPT in ethanol for 18 h at 50 °C, in order to form a densely packed BPT SAM.

(iv) Rinse the BPT SAM sample in ethanol and deionized water to remove any physisorbed molecules from the surface.

(v) Following Steps 22–33, load the sample into the TERS instrument and approach the surface with the TERS probe until it generates contact-mode AFM feedback, using the

previously determined approach parameters in Steps 23–33 to minimize the force on (and therefore the damage to) the TERS probe. Use the procedure described in Steps 34–38 to perform confocal Raman imaging around the probe apex in a 2 × 2-μm area, using a pixel size of 80 nm, integration time of 1 s and laser power (at the sample) of ~100 μW.

(vi) Create a hotspot map, using the intensity of the 1,593-cm^{-1} (aromatic C=C stretch, $\nu_{C=C}$) Raman band.

(vii) Select an area of 500 × 500 nm around the hotspot. Perform confocal Raman imaging around the hotspot, using a pixel size of 20 nm and integration time of 1 s. Create a new hotspot map, using the 1,593-cm^{-1} Raman band intensity.

(viii) Measure a TERS spectrum at the position of new hotspot with an integration time of 10 s.

(ix) Retract the TERS probe. Refocus the laser on the same position on the sample and measure a far-field spectrum with an integration time of 10 s.

(x) Process the TERS spectral data as described in Box 1.

(xi) Calculate the S/N ratio of the 1,593-cm^{-1} BPT Raman band.

(D) **Monitoring of the pNTP → DMAB photocatalytic process using TERS ● Timing 8 h**

(i) Clean a glass coverslip by sonicating in IPA for 20 min, drying it using a flow of N_2 or Ar and finally placing it in a UV–ozone cleaner for 15 min. Allow the UV–ozone cleaner to cool for at least 15 min before removing the coverslip.

(ii) Deposit 3 nm of Cr, followed by a 10-nm Au layer, on a clean glass coverslip via thermal evaporation as described in Steps 5–8.

(iii) Prepare a SAM of pNTP by immersing the Cr–Au-coated coverslip in a 9 mM solution of pNTP in ethanol for 24 h. Rinse the pNTP SAM sample with copious amounts of ethanol and deionized water to remove any surface residuals. Dry the sample under vacuum.

(iv) Install a 633-nm excitation laser (in addition to the 532-nm laser) in the TERS system and ensure that both lasers are well aligned with a diffraction-limited focal spot at the sample. Check the alignment of both 532- and 633-nm lasers by following Steps 12–21.

(v) Following Steps 22–33, bring an Ag-coated TERS probe into contact with the sample and align the probe to the 633-nm laser. Using the 633-nm laser, locate the TERS hotspot by means of the pNTP band at 1,335 cm^{-1} (nitro-group symmetric stretch, $\nu_{NO2,\ sym}$), as described in Steps 34–38.

(vi) At the position of the hotspot, measure time-series TERS spectra (5-s integration time at intervals of 1 s) of the pATP SAM, using 633-nm laser for 90 s.

(vii) Turn off the 633-nm excitation laser and turn on the 532-nm excitation laser. Illuminate the pNTP SAM sample for 30 s to induce the pNTP → DMAB reaction.

(viii) Turn off the 532-nm laser and turn on the 633-nm laser again. Measure the time-series TERS spectra of DMAB (generated in step (vii)) for 5 min.

(ix) Process the TERS spectral data as described in Box 1.

(E) **Nanoscale imaging of a pATP → DMAB photocatalytic reaction using TERS ● Timing 6 h**

(i) Clean a glass coverslip by sonicating it in IPA for 20 min, drying it using a flow of N_2 or Ar and finally placing it in a UV–ozone cleaner for 15 min. Allow the UV–ozone cleaner to cool for at least 15 min before removing the coverslip.

(ii) Deposit a 10-nm layer of Ag directly onto a clean glass coverslip via thermal evaporation as described in Steps 5–8.

(iii) Prepare a SAM of pATP molecules on the Ag substrate by immersing it in a 5 mM solution of pATP in ethanol for 2 h. Rinse the pATP SAM sample with copious amounts of ethanol and deionized water to remove any surface residuals. Dry the sample using N_2 or Ar gas.

(iv) Following Steps 22–33, load the sample into the TERS instrument and approach the surface with the TERS probe until it generates contact-mode AFM feedback, using the previously determined approach parameters in Steps 23–33 to minimize the force on (and therefore the damage to) the TERS probe. Use the procedure described in Steps 34–38 to perform confocal Raman imaging around the probe apex in a 2 × 2-μm area, using a pixel size of 80 nm, integration time of 1 s and laser power (at the sample) of ~100 μW.

(v) Perform TERS imaging for a 200 × 200-nm area by moving the sample in 10-nm steps while keeping the objective lens and TERS probe stationary and measuring a TERS spectrum at each pixel.

(vi) Process the TERS spectral data as described in Box 1.

(vii) Generate a TERS image of the pATP → DMAB reaction on the sample surface, using the fitted intensity of the 1,142-cm^{-1} DMAB Raman band.

▲ CRITICAL STEP Because the pATP → DMAB reaction may take place on the Ag-coated TERS probe as well as on the Ag sample, care must be taken when interpreting the data generated. If there is a possibility of chemical interference by the TERS probe, we recommend protecting the Ag surface of the probe by using an additional dielectric coating[68,97].

(F) **Imaging of newly synthesized phospholipid molecules in biological cells using TERS** ● Timing **6 d**

(i) Seed mouse preadipocytes on 13-mm plastic coverslips in 24-well plates and incubate for 24 h.

(ii) Treat the cells with 10 μM deuterated stearate (prepared by neutralizing DSA with sodium hydroxide) for 6 h. Wash the cells with PBS buffer and fix at room temperature for 20 min in a solution of 4% (wt/vol) paraformaldehyde and 1% (wt/vol) glutaraldehyde in 100 mM PIPES (pH 7.4) warmed to 37 °C.

(iii) Perform a secondary fixation in 2.5% (wt/vol) glutaraldehyde in 100 mM PIPES for 1 h at room temperature. Leave the cells at 4 °C overnight.

(iv) The next day, wash the cell samples three times for 10 min each with 100 mM PIPES, followed by osmication with 1% (wt/vol) osmium tetroxide in 100 mM PIPES for 1 h and washing in deionized water for 20 min.

(v) Wash the cells through a graded ethanol series, first at 50% ethanol for 15 min, then 70% ethanol overnight at 4 °C, then 90% ethanol for 15 min, then 95% ethanol for 15 min and finally 100% ethanol for 2 h, with three solution changes during this time.

(vi) Gradually infiltrate cells with epoxy resin, starting with 25% resin for 1 h, then 50% resin for 2 h, then 75% resin for 1 h and then 100% resin overnight.

(vii) The next day, place the samples in fresh 100% resin two times, for 3 h each time.

(viii) Embed the cells in fresh resin and leave for 24 h at 60 °C for polymerization.

(ix) Remove the plastic coverslip and cut the specimen to obtain thin (1-μm) sections, using an ultramicrotome equipped with a diamond knife.

(x) Clean a glass coverslip by sonicating it in IPA for 20 min, drying it using a flow of N_2 or Ar, and finally placing it in a UV–ozone cleaner for 15 min. Allow the UV–ozone cleaner to cool for at least 15 min before removing the coverslip.

(xi) Mount a thin cell section on the clean glass coverslip and place this on the TERS microscope for nanoscale chemical imaging.

(xii) Create a confocal Raman map of the cell section, using a step size of 1 μm and a spectrum integration time of 10 s per pixel. Identify areas of NSPs, using the intensity of the C–D stretching band at 2,100 cm^{-1}.

(xiii) Following Steps 22–33, approach the surface with the TERS probe near an area of NSPs until the probe generates contact-mode AFM feedback, using the previously determined approach parameters in Steps 23–33 to minimize the force on (and therefore the damage to) the TERS probe. Using the procedure described in Steps 34–38 and the C–D band intensity, perform confocal Raman imaging around the probe apex in a 2 × 2-μm area, using a pixel size of 80 nm, integration time of 1 s and laser power (at the sample) of ~100 μW.

(xiv) Perform TERS mapping of a 1 × 1-μm area, using a pixel size of 50 nm and spectrum integration time of 10 s.

(xv) Process the TERS spectral data to generate a TERS image of NSPs, using the fitted intensity of the C–D band for the data from step (xiv) (see Box 1 for details).

(xvi) In the TERS image, select a 200 × 200-nm area of interest and perform TERS mapping, using a pixel size of 13 nm and spectrum integration time of 10 s.

(xvii) Process the TERS spectral data as described in Box 1 to generate a TERS image of NSPs, using the fitted intensity of the C–D band for the data from step (xvi).

(G) **Nanoscale chemical imaging of SWCNTs in air and water using TERS** ● Timing **12 h**

(i) Clean a glass coverslip in piranha solution and functionalize it with APTES, following the procedure described in the Reagent setup.

(ii) Deposit SWCNTs from a solution of 1% (wt/vol) DOC onto the piranha-cleaned APTES-functionalized glass coverslip.

(iii) Locate an isolated SWCNT on the sample, using CRM.

(iv) Following Steps 22–33, approach the surface with the TERS probe, close to the SWCNT located in step (iii), until the probe generates contact-mode AFM feedback, using the

previously determined approach parameters in Steps 23–33 to minimize the force on (and therefore the damage to) the TERS probe. Use the procedure described in Steps 34–38 to perform confocal Raman imaging around the probe apex in a 2 × 2-μm area, using a pixel size of 80 nm, integration time of 1 s and laser power (at the sample) of ~100 μW.

(v) Perform TERS imaging of the SWCNT, using a pixel size of 10 nm, integration time of 1 s and laser power of ~100 μW.

? TROUBLESHOOTING

(vi) Process the TERS spectral data as described in Box 1. Generate a TERS image, using the fitted intensity of the 1,591-cm^{-1} Raman band (G band).

(vii) Extract a TERS intensity line profile perpendicularly across the SWCNT and calculate the spatial resolution of the TERS image, using Box 1, Step 4.

(viii) For TERS measurement of SWCNTs in water, place a water droplet on top of the SWCNT sample.

(ix) Perform TERS imaging of a SWCNT by following step (iii)–(vi).

(x) Calculate the spatial resolution, using Box 1, Step 4.

Troubleshooting

Troubleshooting advice can be found in Table 1.

Table 1 | Troubleshooting table

Step	Problem	Possible reason	Solution
10	AFM probe does not have a continuous Ag film	AFM probe is not aligned with the direction of Ag vapor rising from the evaporation boat	Adjust the angle of the probe holder, ensuring that the AFM probes face vertically down, directly facing the evaporation boat
37	No hotspot is observed at the TERS probe apex	This could be due to the following reasons: (i) The TERS probe is not plasmonically active due to the degradation of the Ag coating; (ii) The TERS probe is not properly coated with Ag; (iii) Laser alignment of the TERS microscope is not optimal	(i) Ensure that the TERS probes are removed from the inert environment only immediately before use. Furthermore, minimize the exposure time of the TERS probe to the ambient environment; (ii) Use SEM to check the Ag coating of the probe; (iii) Check the laser alignment of the TERS microscope
38	A strong Raman signal for amorphous carbon is observed in the TERS spectrum	This could be due to the following reasons: (i) The laser power is too high, resulting in carbonization of the sample. In the TERS near field, high local temperatures may lead to decomposition of the analyte molecules; (ii) The evaporation chamber is contaminated with organic molecules, leading to contaminated TERS probes	(i) Use a lower laser power for the TERS measurements. Decrease laser power until a TERS spectrum with S/N ≈ 5 is obtained; (ii) Clean the evaporation chamber thoroughly, using three solvents (acetone + ethanol + IPA) for washing, or else use the internal baking procedure described in Step 6
41A(vi)	A strong graphene signal or another signal is observed throughout the TERS map	The graphene flake or some organic molecule (from the sample surface or ambient environment) might have become attached to the TERS probe apex. This can be checked by measuring the TERS probe on a clean glass coverslip and checking for the same Raman signal, as described in Step 41A(x)	Replace the TERS probe with a new one. Find another single-layer graphene flake and repeat the procedure for TERS imaging
41G(v)	A strong SWCNT signal or another Raman signal is observed along a single line during TERS imaging, which disappears in the next line	A SWCNT could have been dragged across the surface by the TERS probe or the TERS probe could have picked up organic contamination from the sample surface or the ambient environment	(i) Minimize the force on the SWCNT from the TERS probe by reducing the deflection set point, while maintaining AFM feedback (ii) Ensure the SWCNTs are immobilized on the surface (iii) A TERS probe contaminated with a SWCNT should be discarded and a new probe should be used for further measurements

Timing

Steps 1–3, oxidation of Si AFM probes: 15 h
Step 4, cleaning of oxidized AFM probes: 1.5 h
Steps 5–8, metal deposition: 5 h
Steps 9–11, TERS probe quality check: 1 h
Steps 12–17, laser alignment of the Raman microscope: 2 h
Steps 18–21, laser alignment quality check: 2 h
Steps 22–33, alignment of the TERS probe with the excitation laser: 10 min
Steps 34–38, location of near-field hotspot at TERS probe apex: 20 min
Steps 39 and 40, near-field hotspot quality check: 10 min
Step 41A, performing TERS imaging of a single-layer graphene sample: 8 h
Step 41B, TERS measurement of a PEDOT:PSS thin film on glass: 2 h
Step 41C, TERS measurement of a SAM of BPT on Au: 6 h
Step 41D, monitoring of pNTP → DMAB photocatalytic process using TERS: 8 h
Step 41E, nanoscale imaging of pATP → DMAB photocatalytic reaction using TERS: 6 h
Step 41F, imaging of newly synthesized phospholipid molecules in biological cells using TERS: 6 d
Step 41G, nanoscale chemical imaging of SWCNTs in air and water using TERS: 12 h
Box 1, processing of TERS spectral and imaging data: 1–2 h

Anticipated results

Overall, we expect a strong enhancement of Raman signals in the near field of Ag-coated TERS probes from samples of varying chemical composition, which would enable observation of molecular details at the nanometer scale. Here we briefly describe example data for the experimental procedures described in the different options of Step 41.

Step 41(A)

In the confocal Raman image of single-layer graphene, a D-band signal may be observed from the edge of the flakes. However, the distribution of the D-band intensity should be diffraction limited, precluding the sharp detection of the graphene edge. However, in the TERS image of the single-layer graphene flake, a strong D-band intensity localized to the edge should be observed. Any structural defects present within the graphene flake may also become visible via enhanced sensitivity to the D band (refs. [59,60] and Supplementary Fig. 1).

Step 41(B)

In the TERS spectrum of a PEDOT:PSS film, an enhanced signal intensity should be observed as compared with the far-field Raman signal. A plasmonically active TERS probe would provide a TERS signal contrast of >1 (ref. [74] and Supplementary Fig. 2).

Step 41(C)

No BPT Raman signal is expected to be observed from the SAM in the far field because of the low sensitivity of confocal Raman spectroscopy. However, in the TERS spectrum, Raman bands of BPT should become clearly visible. A plasmonically active TERS probe should provide a S/N ratio of >10 for the 1,593-cm^{-1} BPT Raman band (ref. [29] and Supplementary Fig. 3).

Step 41(D)

Characteristic pNTP Raman bands should be observed initially in the time-series TERS spectra measured for 90 s using a 633-nm laser. Irradiation of the sample using the 532-nm laser induces the pNTP → DMAB reaction at the Ag-coated TERS probe apex. Characteristic DMAB Raman bands should then be observed in the time-series TERS spectra measured subsequently using the 633-nm excitation laser (ref. [67] and Supplementary Fig. 4).

Step 41(E)

pATP → DMAB reaction hotspots should be observed on the sample in the TERS image generated from the 1,142-cm^{-1} Raman-band intensity. TERS spectra measured at the reaction hotspot contain distinct azo Raman bands of DMAB in the 1,140- to 1,500-cm^{-1} spectral region[98,99], whereas these

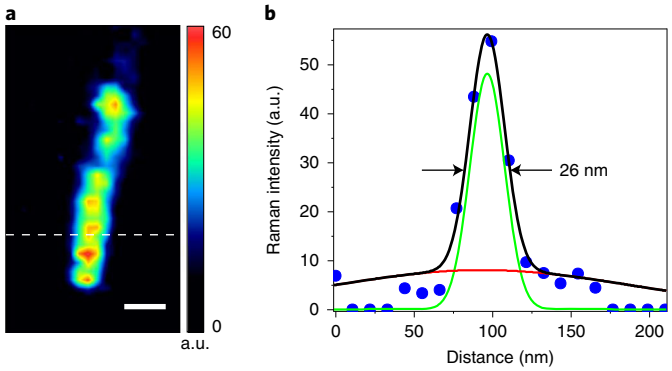

Fig. 8 | Estimating the spatial resolution of a TERS image. a, TERS image of a SWCNT in air, obtained using the 1,591-cm^{-1} Raman band intensity. Scale bar: 50 nm. Integration time for TERS imaging: 1 s; pixel size: 10 nm; laser power at the sample: 170 μW. **b**, Intensity profile along the line marked in **a** with Gaussian curve fits to the near-field (green) and far-field (red) contributions. Spatial resolution of the TERS image is estimated from the FWHM of the green Gaussian curve to be 26 nm. FWHM, full-width at half maximum. Adapted with permission from Kumar et al.[29], Royal Society of Chemistry.

bands should be absent in the TERS spectra measured at other locations on the sample (ref. [68] and Supplementary Fig. 5).

Step 41(F)

NSPs can be visualized in the TERS image of the fitted C–D band intensity, and their nanoscale distribution can be observed. TERS spectra measured at the location of the NSPs clearly show the presence of a C–D band at 2,100 cm^{-1}, whereas the C–D band is expected to be absent in the TERS spectra measured away from them (ref. [52] and Supplementary Fig. 6).

Step 41(G)

SWCNTs should be identified on the sample via their strong Raman signal. Similar nanoscale spatial resolutions are expected to be obtained in the TERS images of SWCNTs measured in air and water, although the SWCNTs imaged in water may show a higher variability in terms of lateral resolution (ref. [29], Fig. 8 and Supplementary Fig. 7).

Reporting Summary

Further information on research design is available in the Nature Research Reporting Summary.

Data availability

The data that support the findings of this study are available from the corresponding author upon reasonable request.

References

1. Kumar, N., Mignuzzi, S., Su, W. & Roy, D. Tip-enhanced Raman spectroscopy: principles and applications. *EPJ Tech. Instrum.* **2**, 9 (2015).
2. Verma, P. Tip-enhanced Raman spectroscopy: technique and recent advances. *Chem. Rev.* **117**, 6447–6466 (2017).
3. Deckert-Gaudig, T., Taguchi, A., Kawata, S. & Deckert, V. Tip-enhanced Raman spectroscopy–from early developments to recent advances. *Chem. Soc. Rev.* **46**, 4077–4110 (2017).
4. Wang, X. et al. Tip-enhanced Raman spectroscopy for surfaces and interfaces. *Chem. Soc. Rev.* **46**, 4020–4041 (2017).
5. Hartschuh, A. Tip-enhanced near-field optical microscopy. *Angew. Chem. Int. Ed. Engl.* **47**, 8178–8191 (2008).
6. Kawata, S. & Shalaev, V. M. *Tip Enhancement* (Elsevier, Amsterdam, 2007).
7. Morton, S. M., Silverstein, D. W. & Jensen, L. Theoretical studies of plasmonics using electronic structure methods. *Chem. Rev.* **111**, 3962–3994 (2011).
8. Weckhuysen, B. M. *In-situ Spectroscopy of Catalysts* (American Scientific Publishers, Stevenson Ranch, 2004).
9. Mestl, G. In situ Raman spectroscopy—a valuable tool to understand operating catalysts. *J. Mol. Catal. A Chem.* **158**, 45–65 (2000).

10. Colthup, N. *Introduction to Infrared and Raman Spectroscopy* (Elsevier, New York, 2012).
11. Perkampus, H.-H. *UV-VIS Spectroscopy and Its Applications* (Springer Science & Business Media, New York, 2013).
12. Kneipp, K., Kneipp, H., Itzkan, I., Dasari, R. R. & Feld, M. S. Ultrasensitive chemical analysis by Raman spectroscopy. *Chem. Rev.* **99**, 2957–2976 (1999).
13. Kim, H., Kosuda, K. M., Van Duyne, R. P. & Stair, P. C. Resonance Raman and surface- and tip-enhanced Raman spectroscopy methods to study solid catalysts and heterogeneous catalytic reactions. *Chem. Soc. Rev.* **39**, 4820–4844 (2010).
14. Cheng, J.-X. & Xie, X. S. Vibrational spectroscopic imaging of living systems: an emerging platform for biology and medicine. *Science* **350**, aaa8870 (2015).
15. Fu, D. et al. Nanoscale infrared imaging of zeolites using photoinduced force microscopy. *Chem. Commun.* **53**, 13012–13014 (2017).
16. Wu, C.-Y. et al. High spatial-resolution mapping of catalytic reactions on single particles. *Nature* **541**, 511–515 (2017).
17. Zhang, R. et al. Chemical mapping of a single molecule by plasmon-enhanced Raman scattering. *Nature* **498**, 82–86 (2013).
18. Zheng, N., Tsai, H. N., Zhang, X., Shedden, K. & Rosania, G. R. The subcellular distribution of small molecules: a meta-analysis. *Mol. Pharm.* **8**, 1611–1618 (2011).
19. Huang, B., Bates, M. & Zhuang, X. Super resolution fluorescence microscopy. *Annu. Rev. Biochem.* **78**, 993–1016 (2009).
20. Hollander, J. M. & Jolly, W. L. X-ray photoelectron spectroscopy. *Acc. Chem. Res.* **3**, 193–200 (1970).
21. Vogt, S. & Lanzirotti, A. Trends in X-ray fluorescence microscopy. *Synchrotron. Radiat. News* **26**, 32–38 (2013).
22. De Jonge, N. & Ross, F. M. Electron microscopy of specimens in liquid. *Nat. Nanotechnol.* **6**, 695–704 (2011).
23. Nuñez, J., Renslow, R., Cliff, J. B. III & Anderton, C. R. NanoSIMS for biological applications: current practices and analyses. *Biointerphases* **13**, 03B301 (2018).
24. Kelly, T. F. & Miller, M. K. Atom probe tomography. *Rev. Sci. Instrum.* **78**, 031101 (2007).
25. Schmid, T., Yeo, B. S., Leong, G., Stadler, J. & Zenobi, R. Performing tip-enhanced Raman spectroscopy in liquids. *J. Raman Spectrosc.* **40**, 1392–1399 (2009).
26. Nakata, A., Nomoto, T., Toyota, T. & Fujinami, M. Tip-enhanced Raman spectroscopy of lipid bilayers in water with an alumina-and silver-coated tungsten tip. *Anal. Sci.* **29**, 865–869 (2013).
27. Scherger, J. D. & Foster, M. D. Tunable, liquid resistant tip-enhanced Raman spectroscopy probes: toward label-free nano-resolved imaging of biological systems. *Langmuir* **33**, 7818–7825 (2017).
28. Martín Sabanés, N., Driessen, L. M. & Domke, K. F. Versatile side-illumination geometry for tip-enhanced Raman spectroscopy at solid/liquid interfaces. *Anal. Chem.* **88**, 7108–7114 (2016).
29. Kumar, N. et al. Nanoscale chemical imaging of solid-liquid interfaces using tip-enhanced Raman spectroscopy. *Nanoscale* **10**, 1815–1824 (2018).
30. Touzalin, T., Dauphin, A. L., Joiret, S., Lucas, I. T. & Maisonhaute, E. Tip-enhanced Raman spectroscopy imaging of opaque samples in organic liquid. *Phys. Chem. Chem. Phys.* **18**, 15510–15513 (2016).
31. Zeng, Z.-C. et al. Electrochemical tip-enhanced Raman spectroscopy. *J. Am. Chem. Soc.* **137**, 11928–11931 (2015).
32. Kurouski, D., Mattei, M. & Van Duyne, R. P. Probing redox reactions at the nanoscale with electrochemical tip-enhanced Raman spectroscopy. *Nano Lett.* **15**, 7956–7962 (2015).
33. Wang, X. et al. Revealing intermolecular interaction and surface restructuring of an aromatic thiol assembling on Au (111) by tip-enhanced Raman spectroscopy. *Anal. Chem.* **88**, 915–921 (2015).
34. Touzalin, T., Joiret, S., Maisonhaute, E. & Lucas, I. T. Complex electron transfer pathway at a microelectrode captured by in situ nanospectroscopy. *Anal. Chem.* **89**, 8974–8980 (2017).
35. Mattei, M. et al. Tip-enhanced Raman voltammetry: coverage dependence and quantitative modeling. *Nano Lett.* **17**, 590–596 (2016).
36. Kumar, N. et al. Simultaneous topographical, electrical and optical microscopy of optoelectronic devices at the nanoscale. *Nanoscale* **9**, 2723–2731 (2017).
37. Liu, Z. et al. Revealing the molecular structure of single-molecule junctions in different conductance states by fishing-mode tip-enhanced Raman spectroscopy. *Nat. Commun.* **2**, 305 (2011).
38. Su, W., Kumar, N., Mignuzzi, S., Crain, J. & Roy, D. Nanoscale mapping of excitonic processes in single-layer MoS_2 using tip-enhanced photoluminescence microscopy. *Nanoscale* **8**, 10564–10569 (2016).
39. Beversluis, M. R., Bouhelier, A. & Novotny, L. Continuum generation from single gold nanostructures through near-field mediated intraband transitions. *Phys. Rev. B* **68**, 115433 (2003).
40. Kumar, N., Kalirai, S., Wain, A. J. & Weckhuysen, B. M. Nanoscale chemical imaging of a single catalyst particle with tip-enhanced fluorescence microscopy. *ChemCatChem* **11**, 417–423 (2019).
41. Hu, D., Micic, M., Klymyshyn, N., Suh, Y. D. & Lu, H. P. Correlated topographic and spectroscopic imaging beyond diffraction limit by atomic force microscopy metallic tip-enhanced near-field fluorescence lifetime microscopy. *Rev. Sci. Instrum.* **74**, 3347–3355 (2003).
42. Neugebauer, U. et al. On the way to nanometer-sized information of the bacterial surface by tip-enhanced Raman spectroscopy. *ChemPhysChem* **7**, 1428–1430 (2006).

43. Cialla, D. et al. Raman to the limit: tip-enhanced Raman spectroscopic investigations of a single tobacco mosaic virus. *J. Raman Spectrosc.* **40**, 240–243 (2009).
44. Najjar, S. et al. Tip-enhanced Raman spectroscopy of combed double-stranded DNA bundles. *J. Phys. Chem. C* **118**, 1174–1181 (2014).
45. Bailo, E. & Deckert, V. Tip-enhanced Raman spectroscopy of single RNA strands: towards a novel direct-sequencing method. *Angew. Chem. Int. Ed. Engl.* **47**, 1658–1661 (2008).
46. Bohme, R. et al. Towards a specific characterisation of components on a cell surface—combined TERS-investigations of lipids and human cells. *J. Raman Spectrosc.* **40**, 1452–1457 (2009).
47. Deckert-Gaudig, T. & Deckert, V. Tip-enhanced Raman scattering studies of histidine on novel silver substrates. *J. Raman Spectrosc.* **40**, 1446–1451 (2009).
48. Blum, C. et al. Understanding tip-enhanced Raman spectra of biological molecules: a combined Raman, SERS and TERS study. *J. Raman Spectrosc.* **43**, 1895–1904 (2012).
49. Yeo, B.-S., Mädler, S., Schmid, T., Zhang, W. & Zenobi, R. Tip-enhanced Raman spectroscopy can see more: the case of cytochrome c. *J. Phys. Chem. C* **112**, 4867–4873 (2008).
50. Davies, H. S. et al. Secondary structure and glycosylation of mucus glycoproteins by Raman spectroscopies. *Anal. Chem.* **88**, 11609–11615 (2016).
51. Lipiec, E., Perez-Guaita, D., Kaderli, J., Wood, B. R. & Zenobi, R. Direct nanospectroscopic verification of the amyloid aggregation pathway. *Angew. Chem. Int. Ed. Engl.* **57**, 8519–8524 (2018).
52. Kumar, N., Drozdz, M. M., Jiang, H., Santos, D. M. & Vaux, D. J. Nanoscale mapping of newly-synthesised phospholipid molecules in a biological cell using tip-enhanced Raman spectroscopy. *Chem. Commun.* **53**, 2451–2454 (2017).
53. Okuno, Y., Saito, Y., Kawata, S. & Verma, P. Tip-enhanced Raman investigation of extremely localized semiconductor-to-metal transition of a carbon nanotube. *Phys. Rev. Lett.* **111**, 216101 (2013).
54. Yano, T.-a et al. Tip-enhanced nano-Raman analytical imaging of locally induced strain distribution in carbon nanotubes. *Nat. Commun.* **4**, 2592 (2013).
55. Yano, T.-A., Verma, P., Saito, Y., Ichimura, T. & Kawata, S. Pressure-assisted tip-enhanced Raman imaging at a resolution of a few nanometres. *Nat. Photonics* **3**, 473–477 (2009).
56. Marquestaut, N. et al. Imaging of single GaN nanowires by tip-enhanced Raman spectroscopy. *J. Raman Spectrosc.* **40**, 1441–1445 (2009).
57. Boehmler, M., Wang, Z., Myalitsin, A., Mews, A. & Hartschuh, A. Optical imaging of CdSe nanowires with nanoscale resolution. *Angew. Chem. Int. Ed. Engl.* **50**, 11536–11538 (2011).
58. Ogawa, Y., Yuasa, Y., Minami, F. & Oda, S. Tip-enhanced Raman mapping of a single Ge nanowire. *Appl. Phys. Lett.* **99**, 053112 (2011).
59. Mignuzzi, S. et al. Probing individual point defects in graphene via near-field Raman scattering. *Nanoscale* **7**, 19413–19418 (2015).
60. Su, W., Kumar, N., Dai, N. & Roy, D. Nanoscale mapping of intrinsic defects in single-layer graphene using tip-enhanced Raman spectroscopy. *Chem. Commun.* **52**, 8227–8230 (2016).
61. Pollard, A. J. et al. Nanoscale optical spectroscopy: an emerging tool for the characterization of graphene and related 2-D materials. *J. Mater. Nanosci.* **1**, 39–49 (2014).
62. Su, W., Kumar, N., Spencer, S. J., Dai, N. & Roy, D. Transforming bilayer MoS_2 into single-layer with strong photoluminescence using UV-ozone oxidation. *Nano Res.* **8**, 3878–3886 (2015).
63. Smithe, K. K. H. et al. Nanoscale heterogeneities in monolayer $MoSe_2$ revealed by correlated scanning probe microscopy and tip-enhanced Raman spectroscopy. *ACS Appl. Nano Mater.* **1**, 572–579 (2018).
64. Park, K.-D. et al. Hybrid tip-enhanced nanospectroscopy and nanoimaging of monolayer WSe_2 with local strain control. *Nano Lett.* **16**, 2621–2627 (2016).
65. Feng, S., Vivian, M., Yao, Z., Dieter, S. A. & Renato, Z. Nanoscale chemical imaging of interfacial monolayers by tip-enhanced Raman spectroscopy. *Angew. Chem. Int. Ed. Engl.* **56**, 9361–9366 (2017).
66. Vivian, M. et al. Structural characterization of a covalent monolayer sheet obtained by two-dimensional polymerization at an air/water interface. *Angew. Chem. Int. Ed. Engl.* **56**, 15262–15266 (2017).
67. van Schrojenstein Lantman, E. M., Deckert-Gaudig, T., Mank, A. J. G., Deckert, V. & Weckhuysen, B. M. Catalytic processes monitored at the nanoscale with tip-enhanced Raman spectroscopy. *Nat. Nanotechnol.* **7**, 583–586 (2012).
68. Kumar, N., Stephanidis, B., Zenobi, R., Wain, A. & Roy, D. Nanoscale mapping of catalytic activity using tip-enhanced Raman spectroscopy. *Nanoscale* **7**, 7133–7137 (2015).
69. Domke, K. F. & Pettinger, B. In situ discrimination between axially complexed and ligand-free co porphyrin on Au(111) with tip-enhanced Raman spectroscopy. *ChemPhysChem* **10**, 1794–1798 (2009).
70. Zhong, J.-H. et al. Probing the electronic and catalytic properties of a bimetallic surface with 3 nm resolution. *Nat. Nanotechnol.* **12**, 132–136 (2017).
71. Hartman, T., Wondergem, C. S., Kumar, N., van den Berg, A. & Weckhuysen, B. M. Surface-and tip-enhanced Raman spectroscopy in catalysis. *J. Phys. Chem. Lett.* **7**, 1570–1584 (2016).
72. Szczerbiński, J., Gyr, L., Kaeslin, J. & Zenobi, R. Plasmon-driven photocatalysis leads to products known from E-beam and X-ray-induced surface chemistry. *Nano Lett.* **18**, 6740–6749 (2018).
73. Wang, X. et al. High-resolution spectroscopic mapping of the chemical contrast from nanometer domains in P3HT:PCBM organic blend films for solar-cell applications. *Adv. Funct. Mater.* **20**, 492–499 (2010).
74. Kumar, N., Rae, A. & Roy, D. Accurate measurement of enhancement factor in tip-enhanced Raman spectroscopy through elimination of far-field artefacts. *Appl. Phys. Lett.* **104**, 123106 (2014).

75. Yeo, B. S., Amstad, E., Schmid, T., Stadler, J. & Zenobi, R. Nanoscale probing of a polymer-blend thin film with tip-enhanced Raman spectroscopy. *Small* **5**, 952–960 (2009).
76. Xue, L *et al. High Resolution Tip Enhanced Raman Mapping on Polymer Thin Films 305* (Wiley-VCH, Weinheim, Germany, 2011). .
77. Saito, Y., Motohashi, M., Hayazawa, N., Iyoki, M. & Kawata, S. Nanoscale characterization of strained silicon by tip-enhanced Raman spectroscope in reflection mode. *Appl. Phys. Lett.* **88**, 143109 (2006).
78. Berweger, S. et al. Optical nanocrystallography with tip-enhanced phonon Raman spectroscopy. *Nat. Nanotechnol.* **4**, 496–499 (2009).
79. Martín Sabanés, N., Ohto, T., Andrienko, D., Nagata, Y. & Domke, K. F. Electrochemical TERS elucidates potential-induced molecular reorientation of adenine/Au(111). *Angew. Chem. Int. Ed. Engl.* **56**, 9796–9801 (2017).
80. Ren, B., Picardi, G., Pettinger, B., Schuster, R. & Ertl, G. Tip-enhanced Raman spectroscopy of benzenethiol adsorbed on Au and Pt single-crystal surfaces. *Angew. Chem. Int. Ed. Engl.* **44**, 139–142 (2005).
81. Blum, C. et al. Tip-enhanced Raman spectroscopy—an interlaboratory reproducibility and comparison study. *J. Raman Spectrosc.* **45**, 22–31 (2014).
82. Wang, X. et al. Revealing intermolecular interaction and surface restructuring of an aromatic thiol assembling on Au(111) by tip-enhanced Raman spectroscopy. *Anal. Chem.* **88**, 915–921 (2016).
83. Huang, T.-X. et al. Tip-enhanced Raman spectroscopy: tip-related issues. *Anal. Bioanal. Chem.* **407**, 8177–8195 (2015).
84. Demming, A. L., Festy, F. & Richards, D. Plasmon resonances on metal tips: understanding tip-enhanced Raman scattering. *J. Chem. Phys.* **122**, 184716 (2005).
85. Yang, Z., Aizpurua, J. & Xu, H. Electromagnetic field enhancement in TERS configurations. *J. Raman Spectrosc.* **40**, 1343–1348 (2009).
86. Yang, L.-K. et al. Rational fabrication of a gold-coated AFM TERS tip by pulsed electrodeposition. *Nanoscale* **7**, 18225–18231 (2015).
87. Meng, L. et al. Gold-coated AFM tips for tip-enhanced Raman spectroscopy: theoretical calculation and experimental demonstration. *Opt. Express* **23**, 13804–13813 (2015).
88. Yeo, B. S., Stadler, J., Schmid, T., Zenobi, R. & Zhang, W. H. Tip-enhanced Raman spectroscopy—its status, challenges and future directions. *Chem. Phys. Lett.* **472**, 1–13 (2009).
89. Kumar, N. et al. Extending the plasmonic lifetime of tip-enhanced Raman spectroscopy probes. *Phys. Chem. Chem. Phys.* **18**, 13710–13716 (2016).
90. Health and Safety Executive. Using nanomaterials at work. in *Health and Safety Executive UK*, *HSG272* (Health and Safety Executive, Bootle, UK, 2013).
91. Yeo, B. S., Schmid, T., Zhang, W. & Zenobi, R. Towards rapid nanoscale chemical analysis using tip-enhanced Raman spectroscopy with Ag-coated dielectric tips. *Anal. Bioanal. Chem.* **387**, 2655–2662 (2007).
92. Cui, X. et al. Tuning the resonance frequency of Ag-coated dielectric tips. *Opt. Express* **15**, 8309–8316 (2007).
93. Taguchi, A. et al. Controlling the plasmon resonance wavelength in metal-coated probe using refractive index modification. *Opt. Express* **17**, 6509–6518 (2009).
94. Hayazawa, N., Yano, T. & Kawata, S. Highly reproducible tip-enhanced Raman scattering using an oxidized and metallized silicon cantilever tip as a tool for everyone. *J. Raman Spectrosc.* **43**, 1177–1182 (2012).
95. Mahan, J. E. *Physical Vapor Deposition of Thin Films* (Wiley-VCH, New York, 2000).
96. Abbe, E. Beiträge zur Theorie des Mikroskops und der mikroskopischen Wahrnehmung. *Arch. Mikrosk. Anat.* **9**, 413–418 (1873).
97. Opilik, L. et al. Chemical production of thin protective coatings on optical nanotips for tip-enhanced Raman spectroscopy. *J. Phys. Chem. C* **120**, 20828–20832 (2016).
98. Huang, Y.-F. et al. When the signal is not from the original molecule to be detected: chemical transformation of para-aminothiophenol on Ag during the SERS measurement. *J. Am. Chem. Soc.* **132**, 9244–9246 (2010).
99. Zhang, Z., Merk, V., Hermanns, A., Unger, W. E. S. & Kneipp, J. Role of metal cations in plasmon-catalyzed oxidation: a case study of p-aminothiophenol dimerization. *ACS Catal.* **7**, 7803–7809 (2017).
100. Buurmans, I. L. C. & Weckhuysen, B. M. Heterogeneities of individual catalyst particles in space and time as monitored by spectroscopy. *Nat. Chem.* **4**, 873–886 (2012).
101. Roy, D., Wang, J. & Williams, C. Novel methodology for estimating the enhancement factor for tip-enhanced Raman spectroscopy. *J. Appl. Phys.* **105**, 013530 (2009).

Acknowledgements

N.K., A.J.W. and A.J.P. acknowledge funding from the National Measurement System of the Department of Business, Energy & Industry Strategy (BEIS), UK. B.M.W. acknowledges support from the Netherlands Center for Multiscale Catalytic Energy Conversion (MCEC), an NWO Gravitation programme funded by the Ministry of Education, Culture and Science of the Government of The Netherlands.

Author contributions

N.K., B.M.W., A.J.W. and A.J.P. conceived and designed the experiments. N.K. collected and analyzed the data. All authors contributed to the discussion and presentation of results and contributed to writing the manuscript.

Competing interests

The authors declare no competing interests.

Additional information

Supplementary information is available for this paper at https://doi.org/10.1038/s41596-019-0132-z.

Reprints and permissions information is available at www.nature.com/reprints.

Correspondence and requests for materials should be addressed to A.J.P.

Publisher's note: Springer Nature remains neutral with regard to jurisdictional claims in published maps and institutional affiliations.

Received: 7 September 2018; Accepted: 9 January 2019;
Published online: 25 March 2019

Related links

Key references using this protocol

Kumar, N. et al. *Nanoscale* **10**, 1815–1824 (2018): https://doi.org/10.1039/c7nr08257f
van Schrojenstein Lantman, E. M., Deckert-Gaudig, T., Mank, A. J. G., Deckert, V. & Weckhuysen, B. M. *Nat. Nanotechnol.* **7**, 583–586 (2012): https://doi.org/10.1038/nnano.2012.131
Kumar, N., Drozdz, M. M., Jiang, H., Santos, D. M. & Vaux, D. J. *Chem. Commun.* **53**, 2451–2454 (2017): https://doi.org/10.1039/C6CC10226C
Mignuzzi, S. et al. *Nanoscale* **7**, 19413–19418 (2015): https://doi.org/10.1039/C5NR04664E

nature research

Corresponding author(s): Andrew Pollard

Reporting Summary

Nature Research wishes to improve the reproducibility of the work that we publish. This form provides structure for consistency and transparency in reporting. For further information on Nature Research policies, see Authors & Referees and the Editorial Policy Checklist.

Statistical parameters

When statistical analyses are reported, confirm that the following items are present in the relevant location (e.g. figure legend, table legend, main text, or Methods section).

n/a	Confirmed	
☐	☒	The exact sample size (*n*) for each experimental group/condition, given as a discrete number and unit of measurement
☐	☒	An indication of whether measurements were taken from distinct samples or whether the same sample was measured repeatedly
☒	☐	The statistical test(s) used AND whether they are one- or two-sided *Only common tests should be described solely by name; describe more complex techniques in the Methods section.*
☒	☐	A description of all covariates tested
☒	☐	A description of any assumptions or corrections, such as tests of normality and adjustment for multiple comparisons
☒	☐	A full description of the statistics including central tendency (e.g. means) or other basic estimates (e.g. regression coefficient) AND variation (e.g. standard deviation) or associated estimates of uncertainty (e.g. confidence intervals)
☒	☐	For null hypothesis testing, the test statistic (e.g. *F*, *t*, *r*) with confidence intervals, effect sizes, degrees of freedom and *P* value noted *Give P values as exact values whenever suitable.*
☒	☐	For Bayesian analysis, information on the choice of priors and Markov chain Monte Carlo settings
☒	☐	For hierarchical and complex designs, identification of the appropriate level for tests and full reporting of outcomes
☒	☐	Estimates of effect sizes (e.g. Cohen's *d*, Pearson's *r*), indicating how they were calculated
☐	☒	Clearly defined error bars *State explicitly what error bars represent (e.g. SD, SE, CI)*

Our web collection on statistics for biologists may be useful.

Software and code

Policy information about availability of computer code

Data collection	TERS data was acquired using a combination of AIST-NT AFM software (HORIBA Scientific, USA) and LabSpec 5 Raman software (HORIBA Scientific, France).
Data analysis	Data analysis was carried out using SPIP, LabSpec 5, OriginPro and MATLAB software.

For manuscripts utilizing custom algorithms or software that are central to the research but not yet described in published literature, software must be made available to editors/reviewers upon request. We strongly encourage code deposition in a community repository (e.g. GitHub). See the Nature Research guidelines for submitting code & software for further information.

Data

Policy information about availability of data

All manuscripts must include a data availability statement. This statement should provide the following information, where applicable:

- Accession codes, unique identifiers, or web links for publicly available datasets
- A list of figures that have associated raw data
- A description of any restrictions on data availability

The data that support the findings of this study are available from the corresponding author upon reasonable request

Field-specific reporting

Please select the best fit for your research. If you are not sure, read the appropriate sections before making your selection.

☒ Life sciences ☐ Behavioural & social sciences ☐ Ecological, evolutionary & environmental sciences

For a reference copy of the document with all sections, see nature.com/authors/policies/ReportingSummary-flat.pdf

Life sciences study design

All studies must disclose on these points even when the disclosure is negative.

Sample size	Only one sample was included here, as a representative example of the anticipated results that can be obtained using the measurement technique.
Data exclusions	No data was excluded as only one representative data set was shown
Replication	No replication is included in this paper, as only a representative image has been used from a previous study.
Randomization	No randomization is included in this paper, as only a representative image has been used from a previous study.
Blinding	Blinding was not relevant to this study which is describing a measurement protocol and anticipated results.

Reporting for specific materials, systems and methods

Materials & experimental systems

n/a	Involved in the study
☒	☐ Unique biological materials
☒	☐ Antibodies
☐	☒ Eukaryotic cell lines
☒	☐ Palaeontology
☒	☐ Animals and other organisms
☒	☐ Human research participants

Methods

n/a	Involved in the study
☒	☐ ChIP-seq
☒	☐ Flow cytometry
☒	☐ MRI-based neuroimaging

Eukaryotic cell lines

Policy information about cell lines

Cell line source(s)	3T3 L1 mouse cells (deriving from Mouse Swiss Albino embryo)
Authentication	None of the cell lines were authenticated
Mycoplasma contamination	Cell lines were not tested for mycoplasma contamination
Commonly misidentified lines (See ICLAC register)	None